UNIVERSITY OF CINCINNATI

Date:_____

I, _____,
hereby submit this work as part of the requirements for the degree of:

_____

in:

_____

It is entitled:

_____

_____

_____

_____

This work and its defense approved by:

Chair: _____

_____

_____

_____

_____

High Strain Functionally Graded Barium Titanate

and its Mathematical Characterization

A dissertation submitted to the

Division of Research and Advanced Studies of the
University of Cincinnati

In partial fulfillment of the
requirements for the degree of

Masters of Science

In the Department of Chemical and Materials Engineering
of the College of Engineering

27th September, 2004

By

Rajesh Surana

B.E., Govt. College of Engineering, Pune, 2000

Committee Chair: Dr. Relva C. Buchanan.

Abstract:

Ferroelectric materials are used in variety of sensor and actuator applications These are generally piezoelectric or electrostrictive, polycrystalline ceramics. The behavior of conventional materials is characterized by good high frequency response and low hysteresis, though the strains are limited to 0.1 %. A variety of methods have been developed for creating large displacement actuators by using monomorph or bimorph benders, RAINBOW, single crystals, relaxor based systems such as PMN-PT, formulated near the morphotropic phase boundary etc. In unimorphs and bimorphs; the bonding interface has low strength. Also large stress discontinuity and concentration are induced in the bonding interface due to the difference of material properties between the shim and piezoelectric material. The stress concentration and structural weakness at the bonding interface are the main causes for the breakdown of the bimorph and unimorph actuators in cyclic actuation. To increase the durability of bending actuators, RAINBOW actuators were proposed. In the RAINBOW, since the reduced layer and piezoelectric layer are chemically integrated, the interface has high strength, but the stress discontinuity cannot be relieved due to the discontinuity of material properties.

In this study more structurally efficient functionally graded barium titanate was investigated. It was found that strain was a function of dielectric constant and spontaneous polarization change; on application of electric field. High dielectric constant was obtained by doping with Nd_2O_3 and ZrO_2, which resulted in core-shell grain microstructure. In addition both grain boundary and surface barrier

structure were used to increase the dielectric constant to the order of 20,000 to 35,000. Due to difference in expansion coefficient of different layers, functionally graded $BaTiO_3$ is pre-stressed and has dome shape. This anisotropic macroscopic stress leads to preferred domain orientation (hence high spontaneous polarization) which when switched by electric field leads to high strain; upto 1.7 %. In this study the following analytical equation was derived to correlate the observations and predict the strain behavior

$$[\Delta e_3]^2 C_{33} = \varepsilon_0 \varepsilon_{33} [\Delta E_3]^2 + \Delta E_3 \Delta P_3^s$$

For dome shaped functionally graded $BaTiO_3$ the effective piezoelectric coefficient, d_{31} calculated was 196 X 10^{-11} C/N and spontaneous polarization change was 0.198 C/m^2. This leads to high strain behavior of functionally graded barium titanate.

Acknowledgement:

This thesis would not have been possible without encouragement, inspiration and constant guidance of my advisor Dr. Relva C. Buchanan. I would like to acknowledge my thesis defense committee members Dr. Ray Lin and Dr. Gregory Beaucage, for their presence and insights in the field of ceramics and materials science. I would also like to acknowledge Dr. Euisuk Park for his co-operation and guidance during initial period of my research. I sincerely appreciate all faculty and staff members, for their co-operation and contribution to my work. I also thank my fellow group members Mr. Ameya Moghe, Mr. Sher Jung Singh and Mr. Chiyaut Ben for their valuable discussion on my research. Lastly this thesis is dedicated to my parents, sister and brother, who will always be inspiration for my academic and professional growth.

Table of Contents

List of Tables:

List of Figures

Chapter 1

Introduction

1.1 Functionally Graded Materials

Because of their coupled mechanical and electrical properties, piezoelectric ceramics have recently attracted significant attention for their potential application as sensors for monitoring and as actuators for controlling the response of structures. The development of a new class of 'smart' composite materials and adaptive structures with sensory/active capabilities may further improve the performance and reliability of the structure systems. Unimorph and bimorph piezoelectric actuators are used for applications which require large displacement output .Since these actuators are manufactured by bonding one or two piezoelectric layers to a metal shim layer; the bonding interface has low strength. On the other hand, large stress discontinuity and concentration are induced in the bonding interface due to the difference of material properties between the shim and piezoelectric material. The stress concentration and structural weakness at the bonding interface are the main causes for the breakdown of the bimorph and unimorph actuators in cyclic actuation. To increase the durability of bending actuators, RAINBOW actuators were proposed. In the RAINBOW, the shim layer is produced by chemical reduction at high temperatures. Since the shim layer and piezoelectric layer are chemically integrated, the interface has high strength. But the stress discontinuity cannot be relieved due to the discontinuity of material properties.

Recent advances in materials science and engineering, coupled with this ubiquitous necessity to create efficient structural systems, have led to a new class of materials called functionally graded materials (FGMs). FGMs offer many distinct advantages over monolithic materials and traditional composites. By spatially varying the microstructure, the material can be tailored for a particular application to yield optimal, thermal, electrical and mechanical behaviour. Through the use of FGMs, improved fatigue resistance, reduced thermo-electro-elastic property mismatch, interlaminar stress reduction, and more efficient joining techniques can be realized.

FGMs have received considerable attention in recent years. The primary focus has been towards the design of efficient materials suited for aerospace applications, solid oxide fuel cells and energy conversion systems using thermoelectric or thermionic materials [1]. An important application of graded materials is in tribology [2, 3] in order to improve the damage resistance of contact surfaces. Thin films with graded composition play an important role in semiconductor devices [4]. Development of FGM in defence mechanisms such as ceramic armour, thermo-nuclear suits etc is also an area of interest. Smooth transitions in compositional gradients also lead to improved bi-material bonding, allowing better mechanical integrity of the systems. With improved functionality of graded materials, their characterization and optimization pose new challenges. In macrostructural analysis, a study of deformation and stress response of FGMs with different material phase variations in the elastic as well elasto-plastic regime is clearly warranted [5]. A comprehensive overview of the elasto-plastic

characterization of FGMs under thermal cycles can be found in [6, 7]. The response of graded materials under transient loads has been studied in order to distinguish the stress wave propagation in graded materials from layered materials [8, 9]. In [9] a semi-empirical numerical model was developed to include strain-rate effects in the elastic and viscoplastic response. In the microstructural characterization of FGM, combined experimental–numerical investigations have been carried out to determine the material parameters such as elastic and plastic properties and fracture toughness [10–12]. Inverse techniques based on neural network and genetic algorithms have also been proposed to characterize graded materials [13, 14]. Exhaustive micromechanical simulations have been performed on periodic and random FGM microstructures in order to derive effective properties and behaviour under prescribed thermo-mechanical excitations [15–18]. Recently, elasto-plastic stress solutions for thermo-elastic FGMs have been presented using a self-consistent approach [19].

One class of FGM, which is the focus of this investigation, is electro-elastic FGM (active FGM), in that the electro-elastic mismatch between constituent material phases is minimized through continuous gradation. In the present context, an FGM comprises ferroelectric or, in particular, piezoelectric material as the material phases. Such materials find use in electro-mechanical devices, popularly known as *smart systems*. Functionally graded transducers have potential applications in ultra-sonic medical imaging where broadband frequency characteristics (short pulse emission) are desirable. Conventional thin piezoelectric transducers are limited due to narrow-band frequency

characteristics on account of the pulses being emitted at both the surfaces [20]. FGM is a nascent area of research. However, the design of a multi-layered actuator in [21] indicates the importance of functionally graded piezoelectric materials in practical applications. Early notable work in this area includes numerical investigations on the nature of surface waves in piezoelectric FGM plates [24, 25]. Analytical studies are focused mainly on either elastic or electrical gradation [26–30]. In [26] microdisplacement and microstructure characteristics of graded piezoelectric materials have been reported. Few researchers have studied controlled responses of functionally graded plates with bonded actuators [27, 28]. In these cases, only elastic gradation is considered. In [29] exact solutions are derived for electrically graded monomorphs. The results indicate the strong influence of electrical gradation on the stress characteristics and electric field. Numerical investigations for FGM bimorphs have been reported [30] for linear and nonlinear gradation to maximize displacement of the actuator while minimizing the maximum stress. However piezoelectric FGMs are still to be fully mathematically characterized for dielectric constant, spontaneous polarization and anisotropic stress dependence of strain. This thesis attempts the mathematical characterization of the piezoelectrically active FGMs and gives out detailed reasons for its high strain characteristics; under the influence of high electric field. It also investigates the data obtained from previous work of my group members on FGMs. Additionally the relationship between dielectric constant and strain is explained. Thus these high capacitance FGMs differ from

the current materials used for obtaining high strain and hence for comparison an overview of high strain materials and strain magnifying mechanisms is given.

1.2 Research motivations and objectives

- Previous study by group members showed that strain was high for high dielectric constant and high spontaneous polarization materials. Therefore it was necessary for developing equations that relate strain to dielectric constant and spontaneous polarization.

- It was required to produce high dielectric constant materials by combining the core-shell grain microstructure and grain boundary and surface barrier layer structure.

- Also it is important to evaluate bulk properties of material which have functionally graded layers.

- As discussed earlier, drawbacks from unimorphs and bimorphs can be avoided by using more structurally efficient FGMs.

- It was important to investigate other factors that contribute to high strain in $BaTiO_3$ FGMs.

- For complete mathematical modeling it was necessary to evaluate mechanical properties.

- Lastly it was necessary to study effect of dome shape and of pre-stressed condition on strain characteristic.

Chapter 2

Background and Literature Review

2.1. Piezoelectric and Electrostrictive Materials:

Many solid state actuators are based on piezoelectric and electrostrictive materials. The piezoelectricity was first discovered by Pierre and Jacques curie, who first examined the effect in quartz in 1880. The subsequent discovery of ferroelectricity and characterization of ferroelectric materials further extended the number of useful piezoelectric materials available for study and application. Extensive characterization of the new ferroelectric material barium titanate ($BaTiO_3$) was independently undertaken by Wainer and Salmon, Ogawa, Wul and Golman from 1940 to 1943. The new material exhibited unusual dielectric properties including exceptionally high dielectric constant with distinctive temperature and frequency dependence. In following years many researchers modified the compositions of $BaTiO_3$ by adding suitable dopants to tailor the properties of the material for improved temperature stability and enhanced high voltage output. The first piezoelectric transducers based on $BaTiO_3$ ceramics were also developed at this time and implemented for a variety of applications.

In 1950's Jaffe and co-workers examined the lead zirconate-lead Titanate (PZT) solid solution system and found certain compositions exhibited exceptionally strong piezoelectric response. In particular, the maximum response was found for compositions near the morphotropic phase boundary between the rhombohedral and tetragonal phases. Due to this modified PZT ceramics have become the dominant piezoelectric ceramics in various applications. More

recently, the development of PZT-based ternary solid solution systems have allowed for the production of even more responsive materials whose properties can be tailored for a variety of applications.

Kawai and coworkers. discovered in 1969 that certain polymers, most notably polyvinylidene difluoride (PVDF), are piezoelectric when stretched during the fabrication. The development of piezoelectric composite materials systematically studied by Newnham et al. in 1978 allow for the further development of the electromechanical properties. The composite structures, incorporating a piezoelectric ceramic and a passive polymer phase, have been formed in a variety of configurations each precisely designed to meet specific requirements of a particular application.

The relaxor ferroelectric electrostricters are another class of ceramic material, which have become important because of no hysteresis present in strain characteristics. Of the many compositions lead magnesium niobate (PMN), doped with 10 % lead titanate (PT), is most widely used composition for actuator applications. Recent advances in the growth of large high quality single crystals have made these materials even more attractive candidates for a variety of new applications, ranging from high strain actuators to high frequency transducers for medical ultrasound devices. More recently thin films such as zinc oxide (ZnO) and PZT have been developed for microelectromechanical (MEMS) devices.

2.2. An overview of solid state Actuators and their materials:

The various properties relating to the input parameters of electric, magnetic field, stress, heat and light with the output parameters charge/current, magnetization, strain, temperature and light are listed in the in table 1. Conducting and elastic materials which generate current and strain outputs, respectively, with input voltage or stress (diagonal couplings) are sometimes referred to as "trivial" materials. [31]

Table 2.1: Properties which differentiate between smart and trivial materials.

Output \ Input	Charge/ Current	Magnetization	Strain	Temperature	Light
Electric Field	Permittivity Conductivity	Electromagnetic Effect	Converse Piezoelectric Effect	Electrocaloric Effect	Electrooptic Effect
Magnetic Field	Magnetoelectric Effect	Permeability	Magnetostriction	Magnetocaloric Effect	Magnetooptic Effect
Stress	Piezoelectric Effect	Piezomagnetic Effect	Elastic Constants		Photoelastic Effect
Heat	Pyroelectric Effect		Thermal Expansion	Specific Heat	
Light	Photovoltaic Effect		Photostriction		Refractive Index

Diagonal Coupling: ▭   Sensors: Column 2

Off-Diagonal Coupling: Smart Materials   Actuator: Column 4

On the other hand pyroelectric and piezoelectric materials, which generate electric field with the input heat and stress, respectively are called as "smart"

materials. The off-diagonal coupling have corresponding converse effects, the electrocaloric and converse piezoelectric effects so that both "sensing" and "actuating" mechanisms can be realized in the same material.

"Intelligent" materials must possess a "drive/control" or processing function which is adaptive in environmental conditions in addition to their actuator and sensing functions. Photostrictive actuators belong to this category. When illuminated, some ferroelectrics generate high voltage. Since ferroelectric is also piezoelectric, photovoltage produced will induce a strain in the crystal. Hence, this type of material generates drive voltage dependant on the intensity of the incident light, which actuates a mechanical response.

If one could incorporate a somewhat more sophisticated mechanism for making complex decisions to its "intelligence", a wise material might be created. General evolution of a material has been

Trivial $\Longrightarrow$ Smart $\Longrightarrow$ Intelligent $\Longrightarrow$ Wise

A brief overview of different solid state actuators and their materials is given below

2.2.1. Shape Memory Alloys:

Many materials exhibit large mechanical deformation when undergoing a structural phase transition. This phase transition can be induced by temperature, stress, or electric field. In some materials, once the mechanical deformation is induced, some deformation may be retained with the release of the load and applied stress, but the original form can be restored with application of heat. This type of action is called shape memory. A shape memory alloy is thus, capable of

remembering a previously memorized shape. It has to be deformed in its low temperature phase Martensite and subsequently heated to the high temperature phase Austenite, e.g. with an electrical current. This is pseudoplastic behavior which is accompanied by slight strain hardening. The alloy generates a high force of the order of 10^8 N/m^2, during the phase transformation. Thus, it can be used as an actuator in a multitude of different applications. The shape change is not restricted to just pure bending. The most suitable actuation mode has proved to be the linear contraction of a straight wire actuator. In contradiction to the mechanical shape memory effect, the thermal shape memory effect is related to a heat stimulus, with which the Memory-Metal is capable of delivering a high amount of work output per material volume. The martensitic low temperature phase can be deformed similar to pure Tin: it can be bent back and forth without strain hardening. This superelastic behavior for which reversible strain of the order 10% can be obtained with a very small effective modulus, which is several orders of magnitude smaller than the modulus of parent phase. Thus, the risk of breakage of a component made from martensitic NiTinol is significantly lower as for instance in stainless steel. And finally when heated into the austenitic phase, the alloy recovers its initial shape. The metallurgical reason for the martensite deformability is the twinned structure of the low temperature phase: the twin boundaries can be moved without much force and without formation of dislocations, which can be considered as being the initiator of fracture.

These are high strain material but these differ from our system in way that phase transition is used to generate the strain.

2.2.2. MEMS (Microelectromechanical Systems)

Integrated electronic circuitry and Silicon have almost become synonymous. Due to its favorable mechanical properties, silicon can also be micromachined to create microelectromechanical systems. Operation of MEMS is based on electrostatic principles. Pressure and acceleration sensors are produced for applications in medical instrumentation and automobiles. One important example is the acceleration sensor used to trigger an air bag in a automobile crash. The generative force/displacement levels produced by MEMS devices are, however, generally too small to be useful for many actuator applications. [32] These invariably have active layers and silicon substrates, hence the gradation is not smooth instead they have sharp transition region.

2.2.3. Polymers

Different types of polymers like piezoelectric polymers, piezoelectric composites, electrostatically active polymers and elastomers are used as actuator materials. Following section deals with it.

a) Artificial Muscle:

In a manner to the silicon MEMS devices, the operation of polymer film actuators is based on electrostatic principles. The basic design and operation of the polymer film actuator is depicted in figure 2.1. Two polymer films with embedded electrodes are placed adjacent to each other. When three-phase voltages (+V, -V, 0) are applied in succession to every three embedded electrodes in the stator film [figure 2.1 (a)] charges of –Q, +Q, and 0 are induced on the opposing slider film [Figure 2.1(b)]. Then when the three voltages are switched to –V, +V and –

V.[figure 2.1(c)], a repulsive force is generated between the stator and slider films, and an attractive force is generated between the adjacent electrodes on the two films. This produces an electrode pitch displacement (in this case a shift of the slider to the right) [figure 2.1(d)]. The electrostatic force generated increases significantly as the electrode gap is reduced. Generally in above described artificial muscle, a thin film of PET, 12 μm in thickness, is used for the slider, to which a polyimide film with surface line electrodes is laminated which serves as stator. [33]
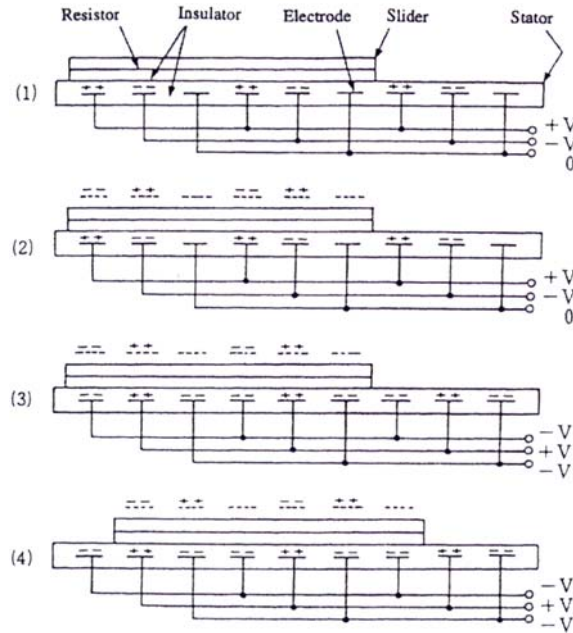
Figure 2.1: The basic design and operation of a polymer film actuator

b) Piezoelectric Polymers:

Polyvinylidene difluoride, PVDF or PVF2, becomes piezoelectric when it is stretched during the curing process. The basic structure of this is depicted in figure 2.2. Thin sheets of the cast polymer are drawn and stretched in the plane of the sheet, in at least one direction, and frequently also in perpendicular

direction, to transform the material to its macroscopically polar phase. Crystallization from the melt produces the nonpolar $\alpha-$ phase which can be converted into the polar $\beta-$ phase by this uniaxial or biaxial drawing operation. The resulting dipole are then realigned by electrically poling the material.
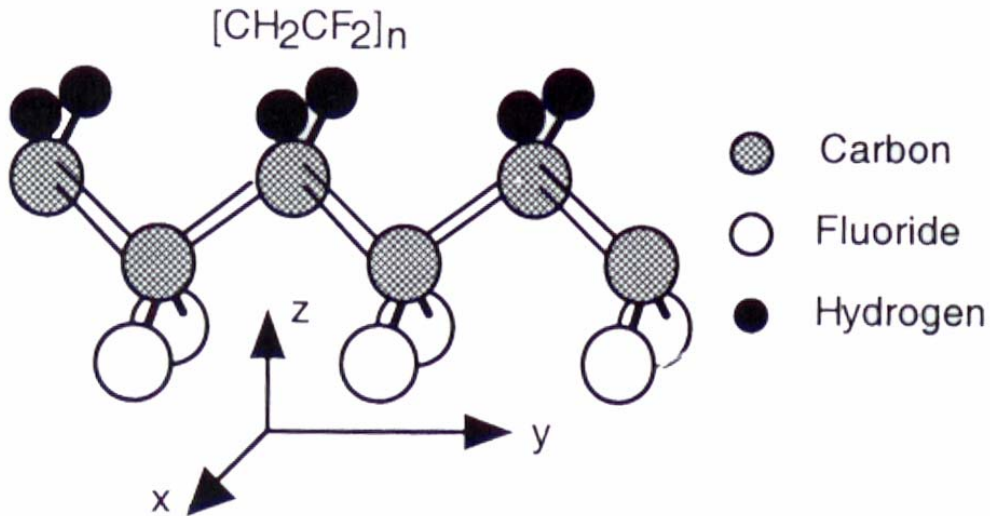
Figure 2.2: Structure of polyvinylidene difluoride (PVDF).

Copolymers of the system polyvinylidene difluoride trifluoroethylene [P(VDF-TrFE)] with a stable polar $\beta-$ phase are well known as piezoelectric materials. The strain induced in this material is not very large, however due to very high coercive field. An electron irradiation treatment has been applied to materials from this system, which significantly enhances the magnitude of the induced strain. Irradiation results in diffuse phase transition and a decrease in the transition temperature as compared with the non-irradiated material. It is believed that the observed changes in the phase transition are due to the development of microdomain state, similar to that associated with relaxor ferroelectrics, which effectively interrupts long range coupling of ferroelectric domains. Induced strains

as large as 5% have been reported. The poled material has a thickness –mode

coupling coefficient, K_t, of 0.30 [34]
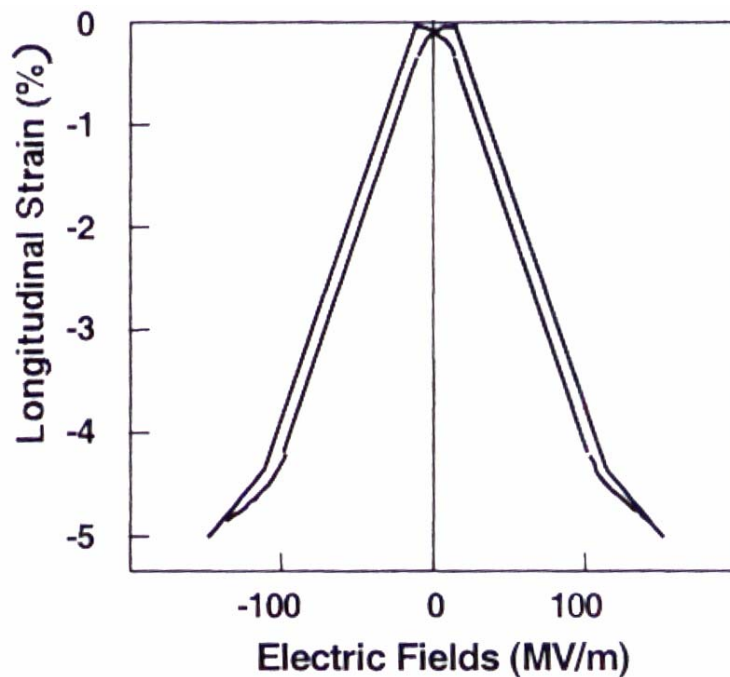
Figure 2.3: The electric field-induced strain curve for an irradiated polyvinylidene difluoride-based copolymer.

Piezoelectric polymers have the following characteristics:

(i)   they have a small piezoelectric strain coefficients, d (for actuatrors) and large g constants (for sensors)

(ii)   they are light weight and elastically soft, allowing for good acoustic impedence matching with water and human tissue,

(iii)   they have low mechanical quality factor, Q_m, allowing for a broad resonance bandwidth.

Piezoelectric polymers are used for directional microphones and ultrasonic hydrophones. The major disadvantage of this materials for actuator applications

are the relatively small generative stress and the considerable heat generation that is generally associated with a low mechanical quality factor.

c) **Piezoelectric composites**:

By using piezoelectric composites the properties can be tailored to suit the particular property by varying the dimensional connectivity. A 1-3 composite shown in figure 2.4 is well known example of this. The advantages of this composite are its high electromechanical coupling factors, good acoustic impedence match to water or human tissue, broad bandwidth and low mechanical quality factor. [35]
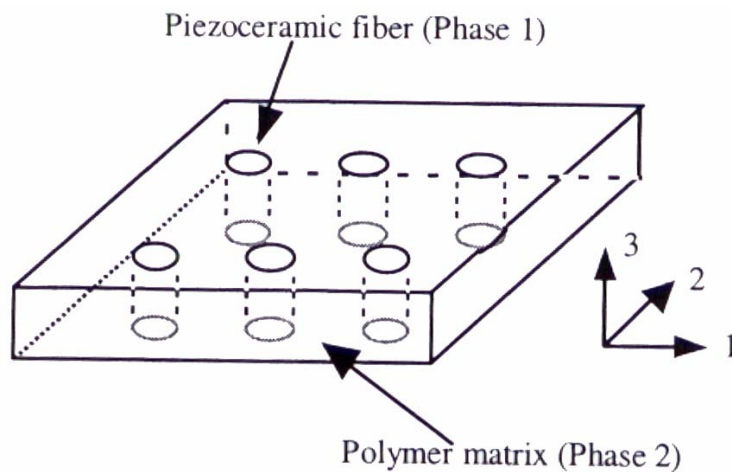
Figure 2.4: A schematic depiction of a 1-3 PZT rod: polymer composite. The top and bottom surfaces are rigid electrodes.

d) **Elastomer actuators:**

Elastomer actuators operate through the Maxwells force that occurs in an electrostatic capacitor. Considering the area, A, and electrode gap,t, filled with dielectric material with a dielectric constant, ε_r, the capacitance, C, and the stored energy, U, will be given by:

$$C = \varepsilon_0 \varepsilon_r \frac{A}{t} \qquad (2.1)$$

$$U = \frac{1}{2} C V^2 \qquad (2.2)$$

Note that an attractive force described by

$$F = \frac{\partial U}{\partial t} = -\frac{1}{2} \varepsilon_0 \varepsilon_r A \left(\frac{V}{t} \right)^2 \qquad (2.3)$$

will be induced between the electrodes, which will lead to a decrease in the interelectrode distance. Hence it can be seen that a larger displacement can be obtained by increasing the compliance and the effective permittivity (and therefore the stored electric charge of the material. A hybrid elastomer was developed whereby a porous PTFE and a stiff PFCB phase are incorporated in a phase as shown in figure 2.5. The stiffer PFCB phase serves to store the charge while porous PTFE phase effectively increases the overall compliance of the structure. [36]
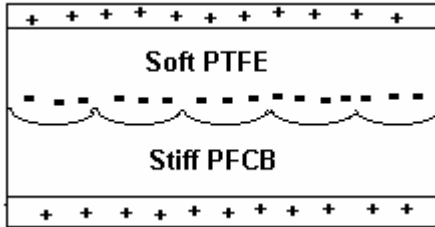
Figure 2.5: Schematic representation of a hybrid elastomer structure incorporating a porous PTFE and a stiff PFCB [36]

These polymer systems are different than the ceramic FGMs except for the fact that Maxwell's equations (equation 2.3) show that the attractive force is proportional to the square of voltage, which is analogous to electrostriction. One similarity as shown equation 3 is dependence of strain on dielectric constant.

2.3. Piezoelectric materials for actuators applications and high strain piezoelectric actuator structures:

Ferroelectric materials are widely used in variety of sensor and actuator aplications. These are generally piezoelectric or electrostrictive, polycrystalline ceramics. Applications in industrial, domestic, military and health care, include micropositioning, ultrasonics, stress measurement, active damping, damage detection, piezoelectric ignition devices and wide aperture electro-optic shutters. The properties of interest for these applications are piezoelectricity and electrostriction. Piezoelectricity, as expressed by the converse piezoelectric effect, is a linear relationship between strain and electric field, while electrostriction is a quadratic relationship [37].

Electric field induced strain curves are shown for piezoelectric lanthanum-doped lead zirconate titanate (PLZT) and elecrtostrictive lead magnesium niobate (PMN) based ceramic in figure 2.6. The piezoelectric response shows the characteristic linear strain versus field relation with a noticeable hysteresis, while the electrostrictive response exhibits no hysteresis and non-linear behavior. Due to this nonlinear behavior, a sophisticated drive circuit is generally needed for electrostrictive actuators.

The behavior of conventional materials is characterized by good high frequency response and low hysteresis, though the strains and stress levels are limited to 0.1% and $4 \times 10^7 \text{N/m}^2$ respectively. A variety of methods have been developed for large displacement by using monomorph or bimorph bender, single crystals, RAINBOW, relaxor based systems such as PMN-PT, formulated near

the morphotropic phase boundary, that take advantage of phase transition to produce actuation strains of greater than 1%.[38]
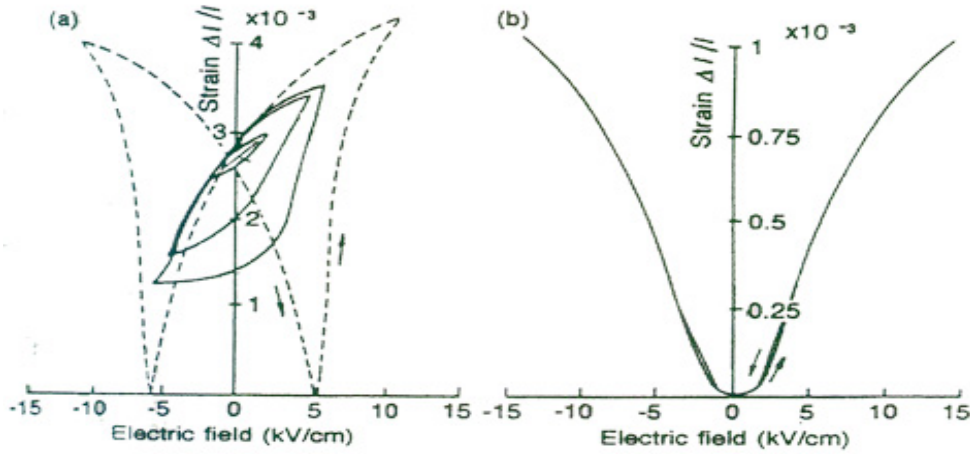
Figure 2.6: Electric field induced strains in a) piezoelectric lanthanum doped lead zirconate titanate and b) elecrtostrictive lead magnesium niobate based ceramic.

Table 2.2: Piezoelectric properties of some popular piezo-materials.

Properties	Quartz	$BaTiO_3$	PZT4	PZT5H	$(Pb,Sm)TiO_3$	PVDF-TrFE
d_{33} (pC/N)	2.3	190	289	593	65	33
g_{33} (mVm/N)	57.8	12.6	26.1	19.7	42	380
k_t	0.09	0.38	0.51	0.50	0.50	0.30
K_p		0.33	0.58	0.65	0.03	
K_{33}^T	5	1700	1300	3400	175	6
Q_m	$>10^5$		500	65	900	3-10
Tc (^{O}C)		120	328	193	355	

2.3.1 Need for piezoelectric actuators

The actual machining apparatus containing translational components (the joints) and rotating components (the gears and motors) introduce error due to mechanical backlash. Machine vibrations also lead to unavoidable position fluctuations. Furthermore the effect of deformation due to machining stress and thermal expansion cannot be ignored. This problems encountered in the conventional machining have led to development of more accurate submicron displacement positioner to improve the cutting accuracy. For example the prototype of lathe having multilayer actuator can achieve cutting accuracy of 0.01 mm^2. [39]

Earlier systems were so designed that parameters like position, angle or the focal lengths of mirror and lens remained essentially fixed during the operation. Newer systems, however, incorporating "adaptive optics" are designed to variety of conditions to essentially adjust the system parameters for optimum operation. . In "LIDAR" system designed by NASA the laser beam is projected towards the earth's surface and the reflected light is received by reflection telescope, amplified by photomultiplier and the resulting signal is processed to produce an image. Here the vibration noise and the temperature difference in space shuttle always posed the obstacle in obtaining the sharp image. The responsive positioner can compensate for this detrimental effect. [39]

The piezoelectric devices also find the extensive use in active and passive vibration suppression. The repeated impact of space dust with the structure like solar panels can severely damage the components. Thus mechanical vibrations

traveling through vacuum of space are not readily damped. Military tanks or submarines use smart skins to minimize the damage of impact of missile on tank or effect of drag force applied to submarine during its motion through turbulent flow in water. The effect of these forces is counteracted by sensing them and then the actuator changing its shape in order to minimize the impact of drag force in submarine. Figure 2.7 illustrates this,
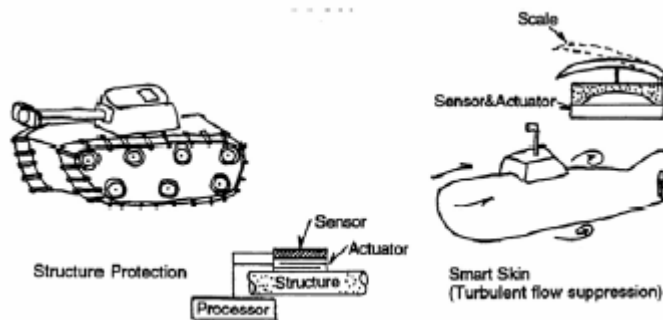
Figure 2.7: Smart skin structures for military tanks and submarines.[39]

Another use that's getting interest and development is "noise control". The active control of sound in aircraft and automobile interiors is a problem that has received considerable attention in the recent past. Active control techniques are typically applied at low frequencies where passive techniques ineffective. Active noise cancellation entails destructive interference or "anti-noise" of sound waves. The most commonly used acoustic source for such applications is the conventional coil and magnet loudspeakers. At low frequencies, such a device tends to get bulky and heavy. The severe weight and space limitations in the design of commercial aircrafts have motivated to look at piezoelectric acoustic noise controllers, as an alternative. [40]

Solid state motors can suffice the ever increasing needs in printers and floppy disk drives. Piezoelectric ultrasonic motors whose efficiency is insensitive to size are superior to conventional devices when motors of millimeter size are required.

2.3.2 High strain piezoelectric actuators structures

The challenges, discussed above, in motion generating devices have led to development of various actuators. Most notably of this are monomorph, unimorphs, bimorphs, rainbow, multilayer actuators etc. Following section deals with basic construction and principle of working.

a) Multilayer Actuators

Ferroelectric ceramic multilayer devices have been investigated intensively for capacitor and actuator applications, because they have low driving voltages and they are highly suitable for miniaturization and integration onto hybrid structures. Miniaturization and hybridization are key concepts in the development of modern micromechatronic systems. The typical layer thickness for multilayer actuators at this time is about 60 µm.

The multilayer structure is essentially comprised of alternating ferroelectric and conducting layers, which are *co-fired* to produce a dense, cohesive unit as shown in Figure 8. A ferroelectric layer sandwiched between a pair of electrodes constitutes a single displacement element. Hundreds of these units may be connected in parallel to the potential difference supplied by the external electrodes, which are connected to the many interleaved internal electrodes of the stack as shown in Figure 2.8.
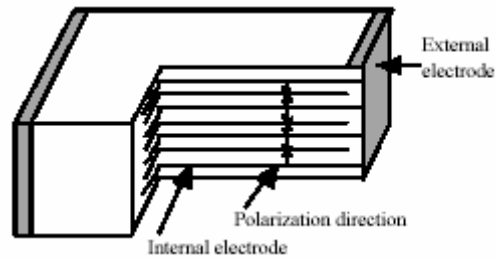
Figure 2.8: The structure of a multilayer actuator.

b) Unimorph/Bimorph

Unimorph and *bimorph* devices are simple structures comprised of ceramic and inactive elastic plates bonded surface to surface. Unimorph devices have one plate and bimorph structures have two ceramic plates bonded onto an elastic *shim*. We will focus on the bimorph structure here. The bending deformation in a bimorph occurs because the two piezoelectric plates are bonded together and each plate produces its own extension or contraction under the applied electric field. This effect is also employed in piezoelectric speakers. The induced voltage associated with the bending deformation of a bimorph has been used in accelerometers. This is a very popular and widely used structure mainly because it is easily fabricated (the two ceramic plates are just bonded with an appropriate resin) and the devices readily produce a large displacement. The drawbacks of this design include a low response speed (1 kHz) and low generative force due to the bending mode. A metallic sheet shim is occasionally used between the two piezoceramic plates to increase the reliability of the bimorph structure as illustrated in figure 2.9.
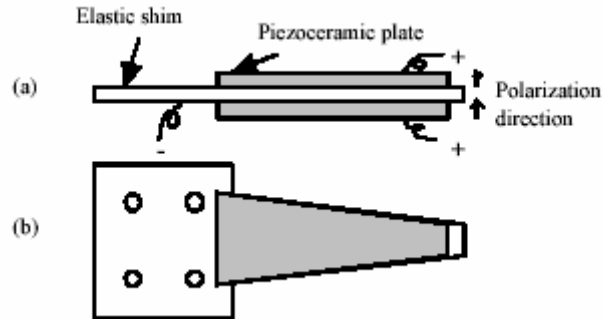
Figure 2.9: Bimorphs with metallic shim layer

When this type of shim is used, the structure will maintain its integrity, even if the ceramic fractures. The bimorph is also generally tapered in order to increase the response frequency while maintaining optimum tip displacement. Anisotropic elastic shims, made from such materials as oriented carbon fiber reinforced plastics, have been used to enhance the displacement magnification rate by a factor of 1.5 as compared to the displacement of a similar device with an isotropic shim.

c) Moonie/Cymbal

A composite actuator structure called the *moonie* has been developed to amplify the pressure sensitivity and the small displacements induced in a piezoelectric ceramic. The moonie has characteristics intermediate between the conventional multilayer and bimorph actuators; it exhibits an order of magnitude larger displacement (100 μm) than the multilayer, and a much larger generative force (10 kgf) with a quicker response (100 μsec) than the bimorph. This device consists of a thin multilayer ceramic element and two metal plates with a narrow moon-shaped cavity bonded together as pictured in Figure 2.10(a). A moonie with dimensions 5(mm)x5(mm)x2.5(mm) can generate a 20 μm displacement

under an applied voltage of 60 V, which is 8 times as large as the generative displacement of a multilayer of similar dimensions. A displacement twice that of the moonie can be obtained with the *cymbal* design pictured in Figure 2.10(b). The generative displacement of this device is quite uniform, showing negligible variation for points extending out from the center of the end cap. Another advantage the cymbal has over the moonie is its relatively simple fabrication. The end caps for this device are made in a single-step punching process that is both more simple and more reproducible than the process involved in making the endcaps for the moonie structure.
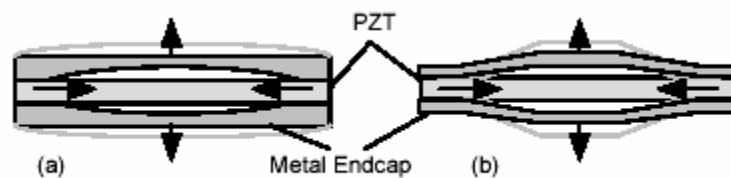
Figure 2.10: Flextensional structures: (a) the moonie and (b) the cymbal.

d) Monomorph

Conventional bimorph bending actuators are composed of two piezoelectric plates, or two piezoelectrics and an elastic shim, bonded together. The bonding layer in the latter, however, causes both an increase in hysteresis and a degradation of the displacement characteristics, as well as delamination problems. Furthermore, the fabrication process for such devices, which involves cutting, polishing, electroding and bonding steps, is rather laborious and costly. Thus, a monolithic bending actuator (*monomorph*) that requires no bonding is a very attractive alternative structure. Such a monomorph device has been produced from a single ceramic plate. The operating principle is based on the

combined action of a semiconductor contact phenomenon and the piezoelectric

or electrostrictive effect. When metal electrodes are applied to both surfaces of a

semiconductor plate and a voltage is applied as shown in Figure 2.11, the

electric field is concentrated on one side (that is, a *Schottky barrier* is formed),

thereby generating a non-uniform field within the plate. When the piezoelectric is

slightly semiconducting, contraction along the surface occurs through the

piezoelectric effect only on the side where the electric field is concentrated. The

nonuniform field distribution generated in the ceramic causes an overall bending

of the entire plate. The energy of a modified structure including a very thin

insulating layer is represented in Figure 2.12a. The thin insulating layer increases

the breakdown voltage.
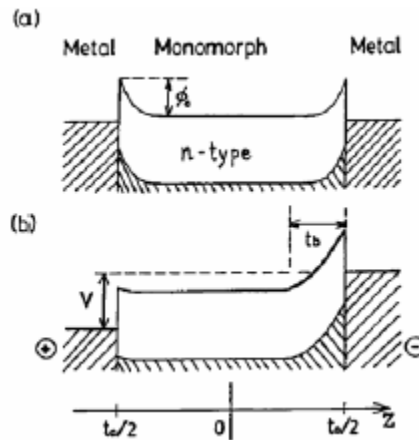
Figure 2.11: Schottky barrier generated at the interface between a semiconductive(n-type) piezoceramic and metal electrodes. Depiction of the energy barrier: (a) before and (b) after the electric field is applied.
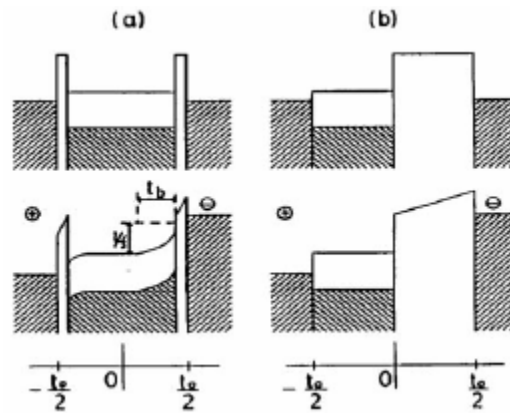
Figure 2.12: Energy diagrams for modified monomorph structures: (a) a device incorporating a very thin insulating layer and (b) the "rainbow" structure.

e) RAINBOW

Recently, a new type of monolithic piezoelectric bending actuator called reduced and internally biased oxide wafer (RAINBOW) device was developed through a special processing technique by Haertling in Clemson University. Comparing with conventional bimorph and unimorph type ceramic benders, RAINBOW actuator demonstrated some unique features: (1) a dome-shaped monolithic composite structure, by which delamination problems usually found in conventional benders can be avoided; (2) larger axial displacement level due to its dome or saddle-like configuration; and (3) higher mechanical strength due to the existence of internal pre-stresses. RAINBOW actuator is fabricated by selectively reducing one surface of high lead-containing piezoelectric materials such as PLZT on flat carbon block at elevated temperature. Optical micrograph of this structure is as shown in figure 2.13. The reduction process of oxide ceramics produces a reduced composite layer with complex composition and phases. It was reported that this reduced layer is composed of metallic lead,

TiO$_2$, ZrO$_2$, ZrTiO$_4$ oxides and reduced PZT or PLZT ceramics. Reactions that take place are shown in figure 2.14. Some metallic lead phase is located intergranularly around other oxide phases, making the reduced layer to show metallic conduction behavior. Since the reduced layer and the remaining PZT or PLZT layer have different thermal expansion coefficients, internal thermal stresses will be generated when materials are cooled down to room temperature after reduction. The change in shape is also believed to be due to reduction in volume of the reduced layer compared to the unreduced layer. The shape of rainbow is shown in figure 2.15. The stress thus originating by single sided reduction process produces a state of tension toward the bottom or reduced side of the wafer and compression towards the top or unreduced side. Therefore the wafer assumes dome or saddle shape, depending on the magnitude of the stress and diameter-to-thickness ratio of the wafer. When both the stress and the diameter-to-thickness are high rainbow takes the higher profile, saddle shape. RAINBOWs can be made into wafer or cantilever type actuators depending on the application requirements. When an electric field is applied across such a composite disc, wafer or cantilever, large axial displacement or tip deflection can be obtained. To optimize RAINBOW actuator performance, a suitable thickness ratio of reduction layer and piezoelectric layer has to be designed. The reduction layer thickness is determined by the thermodynamics and kinetics of the reduction process.
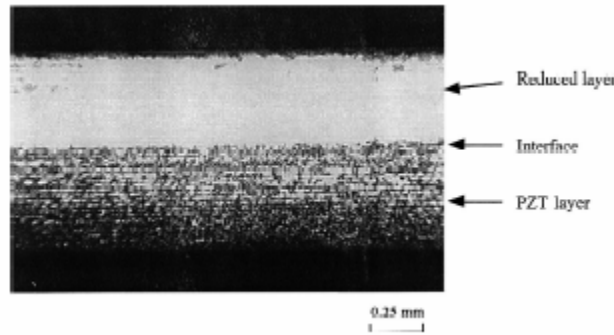
Figure 2.13: Optical Photograph of RAINBOW actuator cross-section.
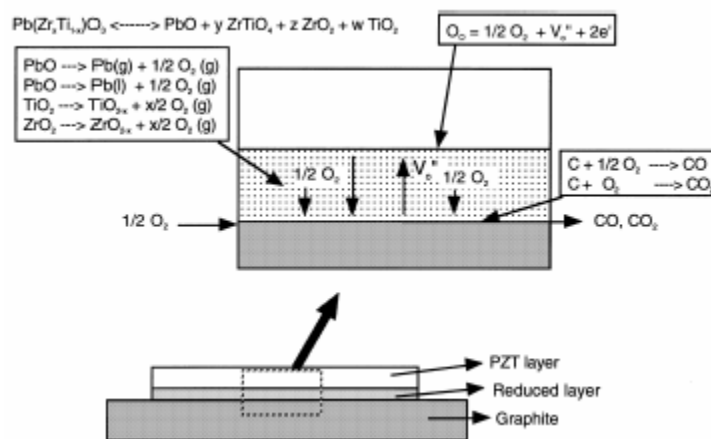
Figure 2.14: Chemical reactions occurring in the fabrication processing of PZT-based RAINBOW actuators.

Figure 2.15: Rainbow Actuator.

Another modification of the basic monomorph structure has been reported made from a $LiNbO_3$ single crystal plate, which has no bonding layer but instead uses an inversion layer generated in the plate. The 500 mm thick z-cut plates were cut from a single domain lithium niobate crystal. Then the unelectroded samples were heat-treated at 1150°C for 5 hours in flowing Ar gas containing water vapor. After rapid cooling at a rate of 50°C per minute, a two-layer domain

configuration structure was created: the spontaneous polarization P_s in the original upward direction in the first layer and an opposing polarization originating from the positive side of the plate in the second. The thickness of the inversion layer depends strongly on the conditions of heat treatment, such as temperature, time and atmosphere. As the annealing temperature or time increases, the inversion layer becomes thicker, and finally reaches the median plane of the plate. After electroding both sides, this single crystal plate will execute a bending deformation with the application of a suitable electric field. Even though the magnitude of the displacement for this device is not as high as a PZT-based bimorph and the actuator is fragile due to crystal cleavage, it has the advantages of a highly linear displacement curve and zero hysteresis.

Though the shape of functionally graded barium titanate is same as RAINBOW, the processing is very different. It does not involve reduction by graphite.

2.4. Barium Titanate:

The perovskite family includes many titanates used in various electroceramic applications, for example, electronic, electro-optical, and electromechanical applications of ceramics. Barium titanate, perovskite structure, is a common ferroelectric material with a high dielectric constant, widely utilized to manufacture electronic components such as mutilayer capacitors (MLCs), PTC thermistors, piezoelectric transducers, and a variety of electro-optic devices [41]. Because of high demands, dielectric characteristics of ceramics materials are rapidly improving. At the same time there have been attempts to reduce the size

of all communication devices as small and as light as possible. Due to this trend, high dielectric constant materials such as barium titanate, with capacity of enhancing temperature stability and dielectric properties by suitable dopant addition, are becoming more important in ceramics materials.

2.4.1. Structure of perovskite-Barium Titanate (BaTiO$_3$)

The perovskite-like structure, named after the CaTiO$_3$ perovskite mineral [42], is a ternary compound of formula ABO$_3$ in which A and B cations differ in size. It is considered an FCC- derivative structure in which the larger A cation and oxygen together form an FCC lattice while the smaller B cation occupies the octahedral interstitial sites in the FCC array. There is only the oxygen being B cation's nearest neighbor. The structure is a network of corner-linked oxygen octahedra, with the smaller cation filling the octahedral holes and the large cation filling the dodecahedral holes [43]. The unit cell of perovskite cubic structure is shown below in Figure 2.16. In Figure 2.16, one can see that the coordination number of A (Ba^{+2} Barium cation) is 12, while the coordination number of B (Ti^{+4}, Titanium cation) is 6. In most cases, the above figure is somewhat idealized [45]. In fact, any structure consisting of the corner-linked oxygen octahedra with a small cation filling the octahedral hole and a large cation (if present) filling the dodecahedral hole is usually regarded as a perovskite, even if the oxygen octahedra are slightly distorted [45]. Also, it is unnecessary that the anion is oxygen. For example, fluoride, chloride, carbide, nitride, hydride and sulfide perovskites are also classified as the perovskite structures. As a result, one can say that perovskite structure has a wide range of substitution of cations A and B,

as well as the anions, if the principles of substitution charge balance are maintained and sizes are within the range for particular coordination number. Because the variation of ionic size and small displacements of atoms that lead to the distortion of the structure and the reduction of symmetry have profound effects on physical properties, perovskite structure materials play important role in dielectric ceramic.
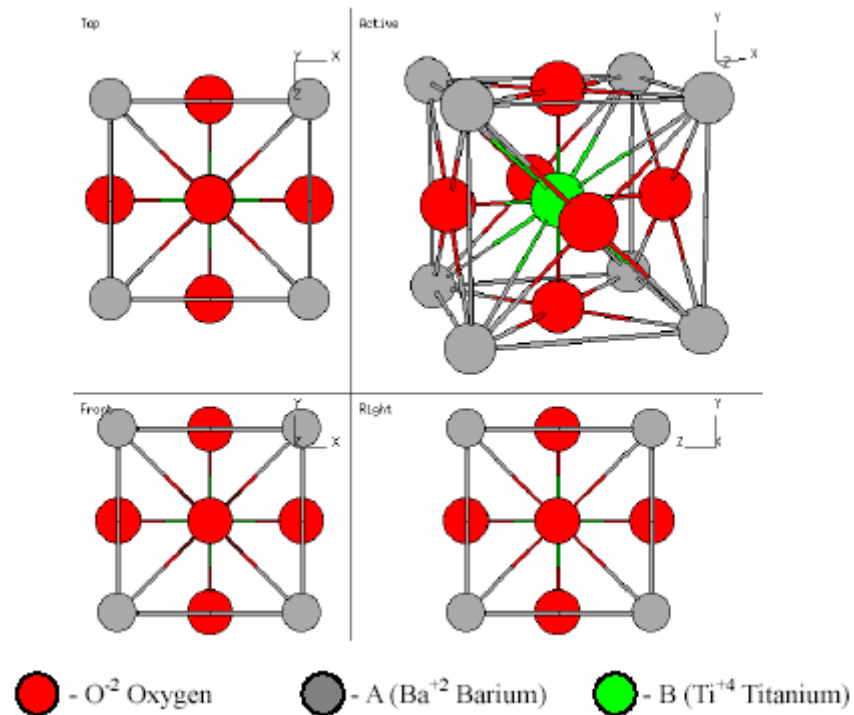
Figure 2.16: Perovskite structure of Barium titanate [44]

2.4.2. Dielectric Characteristics of Barium Titanate

Barium Titanate was the first developed piezoelectric ceramic and even now it is still widely used. It is also a well-known material used for capacitors. The crystallographic dimensions of the barium titanate lattice change with temperature, as shown in Figure 2.17, due to distortion of the TiO_6 octahedra as the temperature is lowered from the high temperature cubic form [49].
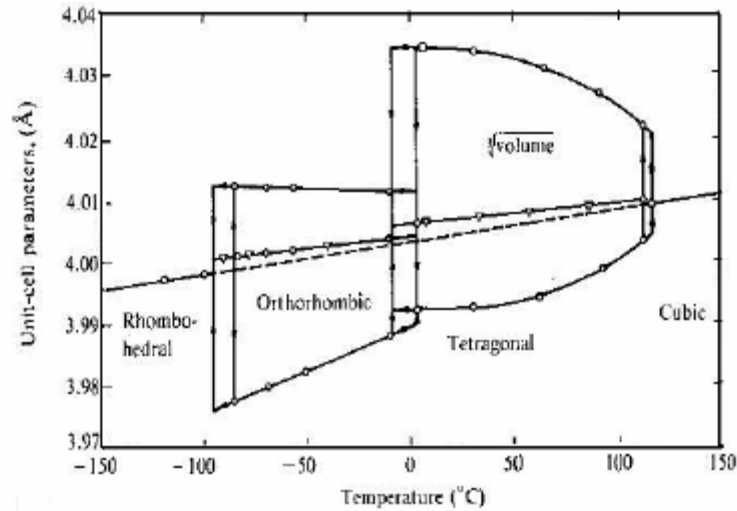
Figure 2.17: Lattice parameters of BaTiO$_3$ as a function of temperature [48]
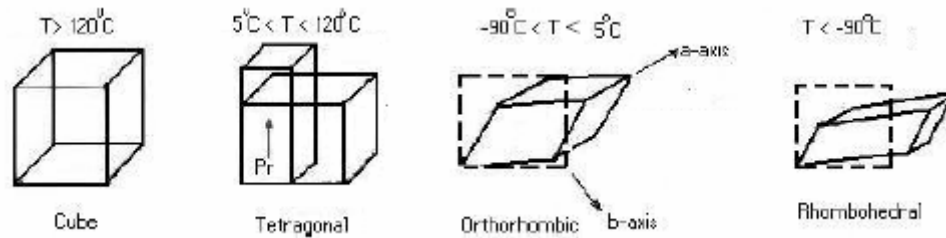
Figure 2.18: Crystallographic changes of BaTiO$_3$ [48]
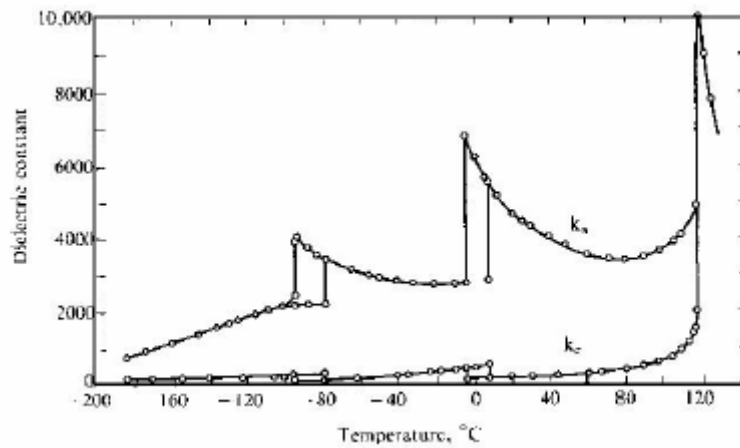
Figure 2.19: Dielectric constants of BaTiO$_3$ as a function of temperature [18]

In figure 2.17 we can see that above 120°C, Curie point Tc, barium titanate ceramic is cubic structure acting isotropic. The Ti atoms are all in equilibrium

positions in the center of their octahedra [41]. Shifting of Ti atom due to applied electric fields could cause the structure to be altered, creating electric dipoles. For example, when temperature is below the Curie temperature, the octahedral structure changes from cubic to tetrahedral symmetry and the position of the titanium ion becomes an off-center position corresponding to a permanent electrical dipole. As the temperature is changed, the crystallographic dimensions change due to distortion of the octahedra resulting in octahedra being coupled together and having a very large spontaneous polarization that leads to a large dielectric constant. These sensitive crystallographic fluctuations with the temperature are shown in Figure 2.18. The dielectric characteristics of barium titanate ceramics with respect to temperature, electric field strength, frequency and time (aging) are also very dependent on the substitution of minor amounts of other ions, on microstructure, and in particular on fine grain size. For example, the room-temperature relative dielectric constant increases as the grain size of the fast-fired $BiTiO_3$ ceramic is decreased [43]. When compared with milling method, chemical mixing techniques show an advantage in enhancing the microhomogeneity of additives, modifying the surface states and then have an effect on the properties of coated ceramics. For instance, in coating process silica is a well-known sintering aid that improves the sintering behavior of $BaTiO_3$ particles and also can produce a core-shell-like structure. By adjusting the core-shell structure, we can control the dielectric properties. The coating process not only can increase the shrinkage rate that improves the sintering behavior but also can inhibits the grain growth.

2.4.3 Domains and domain switching

As discussed earlier at high temperature Barium Titanate has a cubic structure of perovskite, as shown in figure 20. When cooled below 120°C, it transforms to a tetragonal phase. In addition to the strain induced by the lattice distortion, there is a spontaneous polarization along the axis of the unit cell as indicated in the figure 2.20. Thus, at phase transition the unit cell can take any of six crystallographically equivalent combinations of strain and polarization. Furthermore, different regions of a single crystal or single grain in a polycrystal can take on different directions of polarization.
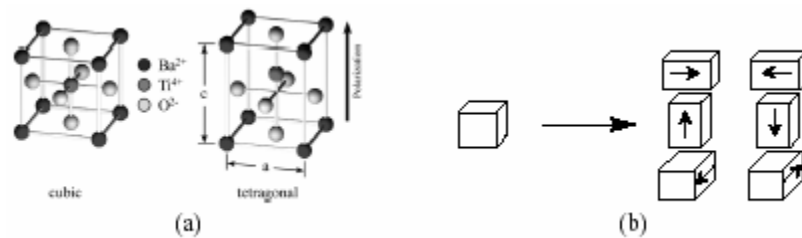
Figure 2.20: (a) The cubic (high temperature) and tetragonal (room temperature) structures of barium titanate. (b) Upon the cubic to tetragonal phase transition, the unit cell can take any of six equivalent combinations of strain and polarization. The arrow indicates the direction of polarization. [37]
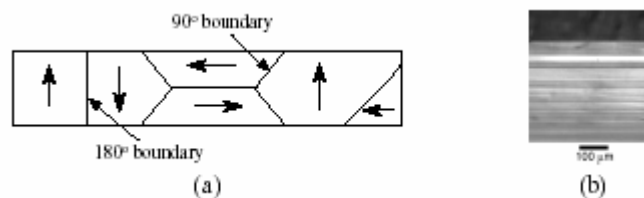
Figure 2.21. (a) Schematic diagram of the subgranular structure of domains separated by 90. and 180. boundaries and (b) a domain pattern photographed using a polarizing microscope.[37]

A region of constant polarization is known as is known as ferroelectric domain. Domains are separated by 90° or 180° domain boundaries, as shown in figure 2.21, which can be nucleated or moved by electric field or stress. The process of

changing the polarization of a domain by nucleation and growth or wall motion is known as domain switching. If the process is induced by electric field, it is known as ferroelectric switching. If it is induced by stress, it is known as **ferroelastic switching.** [37] In a tetragonal unit cell, ferroelectric switching [50] occurs when an applied electric field exceeds the coercive field and thus moves the central ion to another of the six off center tetragonal sites. This changes the direction of polarization to that most closely aligned with the electric field. Same is true for ferroelastic switching (figure 2.22) where direction of polarization aligns in parallel with tensile stress and perpendicular for compressive stress.
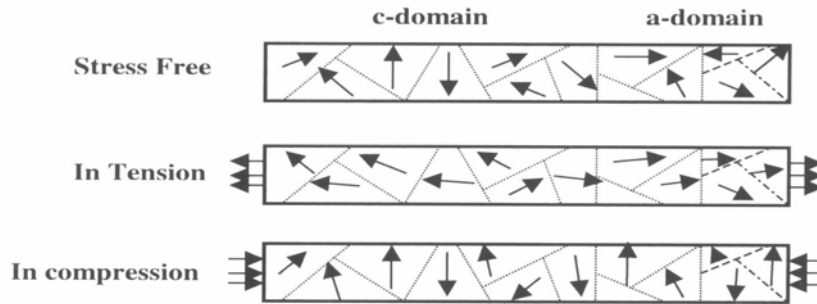
Figure 2.22: Ferroelastic switching [51].

Domain switching is important for number of reasons. Globally it leads to change in the macroscopic polarization direction and in case of 90° domain switching, an associated strain can be quite large – upto 2%. A ferroelectric material must have a direction of average polarization in order to be piezoelectrically active. However the polycrystal, while microscopically polarized, will be macroscopically non-polar due to random orientation of grains and domains. Domain switching makes it possible to pole the material

macroscopically by exposing it to strong field. By the same token piezoelectric material can be depoled by electric field or stress. [52, 53, 54].

2.4.4 Semiconductivity in BaTiO$_3$

Semiconducting BT can be obtained by atmospheric reduction and the formation of oxygen vacancies:

$$O_O \rightarrow \frac{1}{2}O_2 + V_O^{\bullet\bullet} + 2e' \tag{2.4}$$

$$Ti_{Ti} + 2e' \rightarrow Ti_{Ti}^{'} \tag{2.5}$$

or by donor doping, with a trivalent ion (e.g., La^{3+}, Y^{3+}) on the Ba^{2+} site or a pentavalent ion (e.g., Nb^{5+}, Ta^{5+}) on Ti^{4+} site [55]

$$M^{3+} \xrightarrow{\quad BaTiO_3 \quad} M_{Ba}^{\bullet} + Ti_{Ti}^{'} \tag{2.6}$$

$$M^{5+} \xrightarrow{\quad BaTiO_3 \quad} M_{Ti}^{\bullet} + Ti_{Ti}^{'} \tag{2.7}$$

Note that the doping level to create electronic compensation is in general considered at the range from 0.1 to 0.5 atomic %. In both cases above, the substitution is charge compensated by a valency shift for Titanium, providing the shallow donor level (Figure 2.23)

$$e' + Ti_{Ti} \rightarrow Ti^{3+} \Leftrightarrow Ti_{Ti}^{'} \tag{2.8}$$

which has brought up a subject of discussion on the nature of the electrical conduction in n-type BaTiO$_3$.
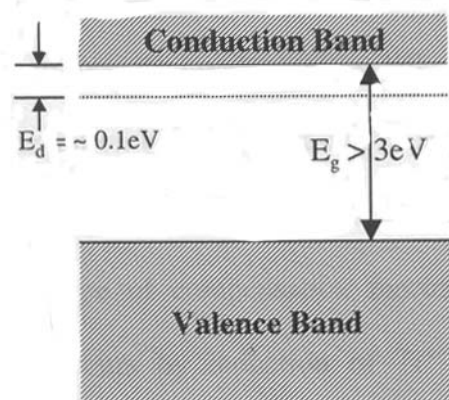
Figure 2.23: Band structure of n-type barium titanate. [56, 57]

Berglund and Braun discovered a broad absorption peak centered at a wavelength of 2 μm in the optical absorption behavior of reduced n-type $BaTiO_3$ but the impurities at this level; within the donor level of approximately 0.2 to 0.3 eV, below the conduction level, were oxygen vacancies[58]. Later Ihrig [59] revealed, from the defect chemistry studies on donor–doped n-type $BaTiO_3$, that there were no impurity or defect levels in the range of 0.1 to 0.8 eV below the conduction band. This indicated that IR-absorbing species might be a charge carrier without "band character", i.e. a polaron. Specific to n-type $BaTiO_3$, the charge carrier is the small polaron and consecutive polaron hops are correlated, reducing the activation energy of hopping, and resulting in the enhanced mobility.

a) Compensation mechanisms in Donor-doped $BaTiO_3$ ceramics:

The electrical conductivity of $BaTiO_3$ prepared by the aliovalent donor doping is extremely sensitive to the concentration and distribution of dopants, and sintering conditions. Small amount of substitution of trivalent donors(e.g. La^{3+}, Y^{3+}, Nd^{3+}) on Ba^{2+} site or pentavalent donors (e.g. Nb^{5+}) on Ti^{4+} site also yields the semiconductivity. A complex defect structure arises as charge compensation

mechanisms further develop. In general, therefore, the conductivity is believed to increase with dopant amount up to a critical concentration before decreasing to an insulting state of bulk $BaTiO_3$ ceramics. In other words, differences in smaller and greater concentrations of donors results in differences in the type of compensation mechanism. That is, for small concentrations compensation occurs by reduction of Ti^{4+} to Ti^{3+}, while for larger concentrations, high donor content, compensation occurs by formation of cation vacancies. At low dopant concentrations (approximately<0.3%), n-type conduction or electronic compensation results from the formation of donor Ti^{3+} ions. At higher dopant concentration, the mechanism changes from electronic to ionic ($[V_{Ti}]$ and/or $[V_{Ba}]$ vacancies) compensation and the resistivity significantly increases. Low resistivities are obtained only within a very narrow dopant concentration range (0.1-0.3 mol%).[56,57]

b) Oxidation effect on Conduction mechanism:

Vacancies in the perovskite lattice can be large in number especially A-sites and moderately so for oxygen vacancies. It is believed that the B-site vacancies ($V_{Ti}^{''''}$) are much lower in concentration and are not as significant. Compositions which might yield B-site vacancies typically crystallize into mixture of phases. Increased diffusion permit easier A-site vacancy compensation of donors, and does occur with higher sintering temperatures and longer firing times, thereby increasing the resistivity. The effect of oxidation, however, has usually been considered separately from donor effects, even though it is highly possible that both donor substitution and oxidation effects can coexist and thus affect the

conduction of BaTiO$_3$ as a combined effect because oxygen also can be regarded as donor or acceptor by interacting with the lattice and thus producing electrons or holes [60].

During the high temperature sintering process loss of oxygen may take place, since oxides can react, often reversibly, with their gaseous environments as following

$$MO \rightarrow MO_{1-x} + \frac{x}{2}O_2\,(gas)\uparrow \qquad (2.9)$$

which in turn results in the slight change in the composition, nonstoichiometry. The very sensitive non-equilibrium conditions, therefore, are developed to some degree. A number of researchers have studied the gas-solid equilibrium between oxides and the atmosphere in which they are fired and the existing boundaries of the various phases are well defined. The phase boundary which describes the atmosphere – temperature relationship can be expressed, in general, as

$$\log Po_2 = -\frac{C_1}{T} + C_2 \qquad (2.10)$$

where C_1 and C_2 are constants in Arrhenius type plot of temperature versus equilibrium oxygen partial pressure. At certain elevated temperature, equilibrium atmosphere exhibits very low pressure. As the temperature drops, equilibrium atmosphere increases rapidly because of Arrhenius-type relationship of equation (2.10). BaTiO$_3$ has been known to experience reduction during high temperature sintering over 1300^OC. [30]

The free electrons created by loss of oxygen in the Barium Titanate lattice contribute to the formation of Ti^{3+} states and thereby to the increase of

conduction. This oxygen nonstoichiometry also causes the color change in the BaTiO$_3$ due to presence of oxygen vacancies produced during high temperature sintering above 1300°C [30]

c) Nonstoichiometry due to oxygen loss in sintering BaTiO$_3$

Considering the reduction reaction given in equations below, defects can be obtained. The formation of electrons under reducing atmosphere is expressed by,

$$O_O \xrightarrow{k_1} \frac{1}{2}O_2 + V_O^{\bullet\bullet} + 2e' \qquad\qquad (2.11)$$

and $[e']=n= 2[V_O^{\bullet\bullet}]$ (2.12)

where an oxygen ion is observed to leave the solid for the gas phase, leaving behind a new positively charged vacant site and two excess electrons. The vacancy can be viewed as a donor defect, producing excess electrons. The equilibrium constant k_1 is expressed by equation (2.13) because $[O_O]$ can be approximated to be 1.

$$k_1 = \log P_{o_2}^{1/2}[V_O^{\bullet\bullet}][e']^2 \qquad\qquad (2.13)$$

Upon change of temperature or atmosphere, oxygen can diffuse out of the lattice during reduction or into the element from the gas phase during oxidation. For latter situation, the oxidation reaction given in terms of the defects can be achieved such that formation of holes under oxidation atmosphere is expressed by

$$\frac{1}{2}O_2 \xrightarrow{k_2} O_O + V_{Ba}'' + 2h \qquad (2.14)$$

and $[h]=p=2[V_{Ba}'']$ \qquad (2.15)

$$\text{or } \frac{1}{2}O_2 + V_O^{\bullet\bullet} + 2e' \xrightarrow{k_3} O_O \qquad (2.16)$$
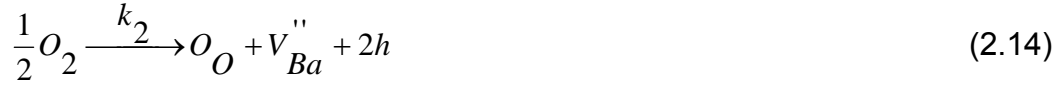
In above equation (2.14) the oxygen is incorporated into rather stoichiometric BaTiO$_3$ lattice from the gas phase, creating a new negatively charged vacant site and two excess holes. The barium vacancy can be viewed as acceptor defect such that

$$null = h + e' \qquad (2.17)$$

The latter equation (2.16) indicates the reversible reaction of equation (2.11) due to reoxidation resulting in the net zero charge in the lattice. It should be noticed that although (e') produced by oxygen loss subsequently forms (Ti$_{Ti}$') polaron as shown in equation (2.5), (2.6) and (2.7), (e') will be used for clarifying the difference from (Ti$_{Ti}$')

d) Donor doping combined with oxidation effect

The substitution of Nd^{3+} in BaTiO$_3$ lattice more likely produces barium vacancy than Titanium vacancy as expressed by equation (2.18)

$$Nd^{3+} \xrightarrow{BaTiO_3} Nd_{Ba}^{\bullet} + \frac{1}{2}V_{Ba}'' \qquad (2.18)$$

and polaron by

$$Nd^{3+} \xrightarrow{BaTiO_3} Nd_{Ba}^{\bullet} + Ti_{Ti}' \qquad (2.19)$$

Note that equation (2.18) applies for donor doping content far above the resistivity minima region according to literature. Therefore total negative charge in the system is given as sum of Equation (2.18), (2.19) and (2.11) by taking into account all possibilities.

$$[NegativeCh\arg e]_{net} = \frac{1}{2}[V_{Ba}^{''}] + 2[e'] + [Ti_{Ti}^{'}] \qquad (2.20)$$

When the concentration of oxygen vacancy is dominated by eqn (2.11) the following relation is derived;

$$[NegativeCh\arg e]_{net} = [e'] \qquad (2.21)$$

Therefore substitution of equation (2.11) into equation (2.20) yields equation (2.22)

$$[e'] = (2k_1)^{1/3} P_{O_2}^{-1/6} \qquad (2.22)$$

When the concentration of cation vacancy is dominated by equation (2.18) in the ionic compensation region as typically proposed by many researchers, the following relation is derived

$$[NegativeCh\arg e]_{net} = [V_{Ba}^{''}] \qquad (2.23)$$

It implies that $[V_{Ba}^{''}]$ is independent of oxygen partial pressure. Lastly, the compensation mechanism around the conduction maximum is known to be polaron conduction of $[Ti_{Ti}^{'}]$, such that

$$[NegativeCh\arg e]_{net} = [Ti_{Ti}^{'}] \qquad (2.24)$$

2.5 Principles of Dielectrics

Dielectrics and insulators can be defined as materials with high electrical resistivities [46]. A good dielectric is, of course, necessarily a good insulator, but the converse is by no means true [46]. Dielectric properties, dielectric constant, dielectric loss factor, dielectric resistivity, and dielectric strength are interpreted as follows.

2.5.1. Capacitance: The principal characteristic of a capacitor is that an electrical charge Q can be stored [40]. The charge on a capacitor is given in equation 2.25,

$$Q=CV \qquad\qquad\qquad (2.25)$$

where V is the applied voltage and C is the capacitance [17]. The capacitance C contains both a geometrical and a material factor [17]. For a large plate capacitor of area A and thickness d the geometrical capacitance in vacuum is given by Equation 2.26

$$C0=(A/d)\varepsilon_0 \qquad\qquad\qquad (2.26)$$

where ε_0 is the permittivity (dielectric constant) of a vacuum [48]. If a ceramic material of permittivity ε' is inserted between the capacitor plates,

$$C=C0^*(\varepsilon'/\varepsilon_0)=C_0.\varepsilon_r \qquad\qquad\qquad (2.27)$$

where ε_r is the relative permittivity or relative dielectric constant, then the capacitance can be shown in Equation 2.27. This is the material property that determines the capacitance of a circuit element.

2.5.2 Dielectric loss factor: The loss factor ε'' is the primary criterion for the usefulness of a dielectric as an insulator material [18].

$$\varepsilon'' = \tan\delta / \varepsilon' \hspace{4cm} (2.28)$$

In equation (2.28), ε' is dielectric constant defined above, while $\tan\delta$ is the dissipation factor. For this purpose it is desirable to have a low dielectric constant and particularly a very small loss angle [48]. Applications that are desirable to obtain a high capacitor in the smallest physical space, the high dielectric constant materials must be used and it is equally important to have a low value for the dissipation factor, $\tan\delta$ [48].

2.5.3. Dielectric strength: Dielectric strength is defined when the electric field is just sufficient to initiate breakdown of the dielectric [46]. It depends markedly on material homogeneity, specimen geometry, electrode shape and disposition, stress mode (DC, AC or pulsed) and ambient conditions [46].

2.6. Barrier layer structures:

Ceramic capacitive components must have high permittivity for volumetric and low temperature coefficient of capacitance for circuit performance. These capacitors are based on ferroelectric compounds such as $BaTiO_3$ in which desirable dielectric properties are obtained by isovalent or aliovalent cation substitution into the perovskite lattice. In small concentrations, substitutions of NiO, ZrO_2, Dy_2O_3 and Nb_2O_3 may also act as grain size inhibitors [61-62]. These oxides modify the ferroelectric properties by controlling the grain size and by suppressing or broadening the curie peak. The dielectric properties of the $BaTiO_3$ have been shown to be very grain size dependent. Fine grained $BaTiO_3$ exhibits permittivity of 3500 to 4000 at room temperature and values approaching to 6000 have been reported, alongwith general broadening of peak transition [63-68].

Additionally it was determined from x-ray diffraction analysis that the degree of tetragonality can be reduced with the decrease in grain size, giving rise to pseudocubic structure at room temperature. For this predominantly line broadening effects, rather than distinct structural changes, are observed in the X-ray profile.

Additionally to meet the temperature required temperature dependence of the dielectric constant, effects of stress as well as presence of chemically in homogeneous grain can be used.[69-71] The chemical inhomogeneous grain consists of three parts: grain core, concentration gradient region and grain shell. Since in situ TEM study, it has become apparent that

i) the temperature dependence of the dielectric constant relates to the chemically inhomogeneous grain (so called compositionally inhomogenity)

ii) that domain pattern's change of the grain core exhibits the three ferroelectric transitions of pure $BaTiO_3$ with respect to temperature

iii) and that grain core and grain shell were not different phases.

Then temperature dependence may take the Lichtenecker type average of the three regions: grain-core, grain shell and concentration gradient region.

When $BaTIO_3$ cools through the ferroelectric transition (Tc) it undergoes a phase transition from cubic to tetragonal. Accompanying this phase change is a volume expansion (~1.0 %) which can lead to the development of complex stress state. It has been suggested that the stress system of grain-core may consist of compression along c-axis, tensile stress along two a-axes, or a combination of the two. Because this stress would suppress the spontaneous deformation of

tetragonal unit cell, forcing it to become more cubic, the temperature dependence of the dielectric constant is depressed and the three transition temperatures (T_c, T_1 and T_2) are shifted. This type of core shell microstructures are both observed in ZrO_2 and Cerium modified barium titanate. Grain boundary Barrier layer capacitors (GBBLC) use this modified core shell structures. In GBBLC, figure 2.24, the semiconducting grains are surrounded by insulating layer in the grain boundary.
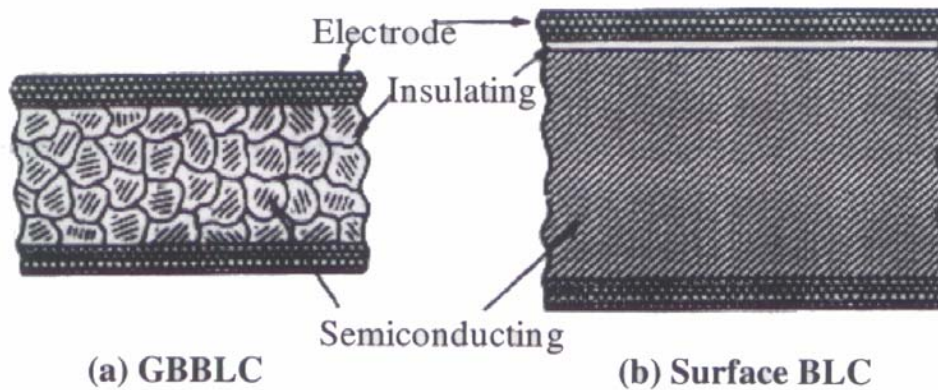
Figure 2.24: Barrier layer capacitors (a) Grain boundary barrier layer capacitor and (b) Surface barrier layer capacitor [61].

The anomalously high permittivity is explained in terms of space charge enhancement, which can be calculated in terms of limiting case of semiconducting grain thickness to insulating boundary width. The brick model illustrated in figure 26 is the most accepted model for GBBLC. When the acceptor paste is coated on a semiconducting ceramic and diffused into the grain boundaries, the boundary layer becomes highly resistive. In figure 2.25, the GBBLC is composed of many cubic units of a grain size D with a resistive skin of

dielectric constant ε_s and δ (skin thickness) which is half the grain boundary thickness.
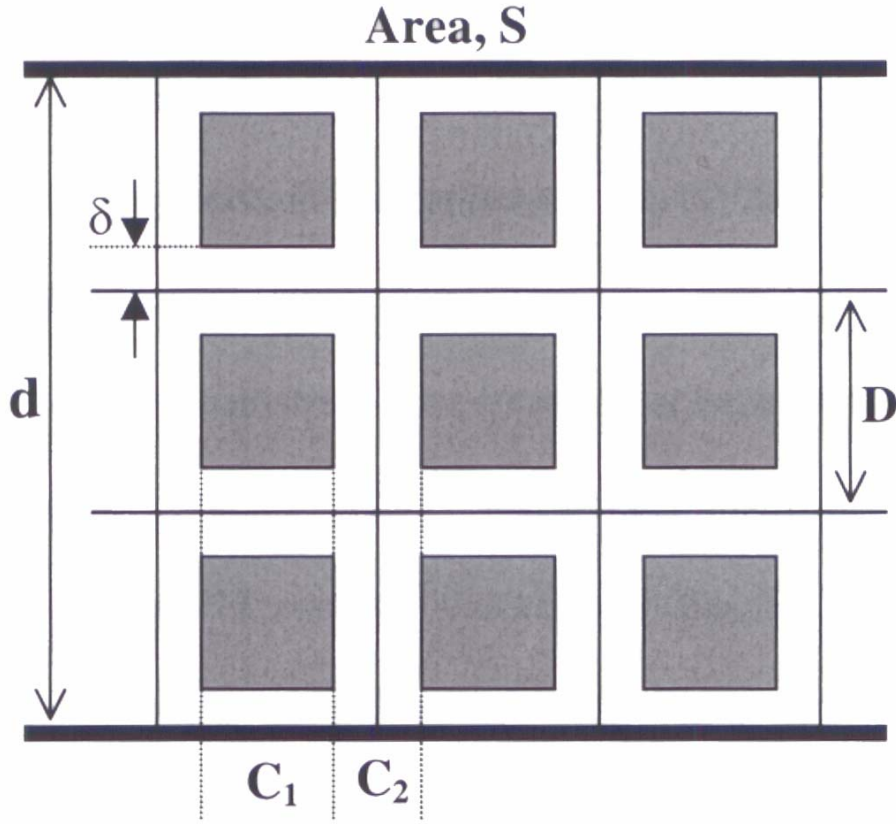
Figure 2.25: Brick model of GBBLC capacitor[72]

The capacitor in figure 2.25 can be divided into two regions C_1 and C_2. In the case of C_1, the area $\left[S-(D-2\delta)^2(S/D^2)\right]$ and the thickness are and d respectively such that

$$C_1 = \varepsilon_0\varepsilon_s\left(\frac{S}{d}\right)\left[1-\left(1-2\frac{\delta}{D}\right)^2\right] \qquad (2.29)$$

$$= \varepsilon_0\varepsilon_s\left(\frac{S}{d}\right)\left(\frac{4\delta}{D}\right) \qquad \left(\frac{\delta}{D}\right) << 1 \qquad (2.30)$$

Also in case of C_2, a capacitor connected in series with an area $(D-2\delta)^2(S/D^2)$ and thickness 2δ, such that

$$C_2 = \left(\frac{D}{d}\right)\varepsilon_0\varepsilon_s \frac{\left[S\left(1-2\dfrac{\delta}{D}\right)^2\right]}{2\delta} \tag{2.31}$$

$$= \varepsilon_0\varepsilon_s \left(\frac{S}{d}\right)\left(\frac{D}{2\delta}\right) \qquad\qquad \left(\frac{\delta}{D}\right) << 1 \tag{2.32}$$

While in surface barrier layer capacitors the thin insulating layer formed just beneath the electrode leads to a large apparent dielectric constant. In order to understand the determining parameters of effective permittivity, the microstructure as shown in figure 2.24b have been modeled using the equivalent circuit (figure 2.26). Since all the layers in surface barrier layer capacitor are horizontal to the electrodes, the structure corresponds to capacitive elements in series and the inverse capacitances are additives, resulting in the following equations:

$$\frac{1}{C_{tot}} = \frac{1}{C_1} + \frac{1}{C_2} + \frac{1}{C_1} \tag{2.33}$$

assuming that two oxidized layers exhibit the dielectric behavior. Therefore the dielectric constants for two regions

$$C_1 = \varepsilon_0\varepsilon_{r_1}\frac{A}{d_1} \tag{2.34}$$

$$C_2 = \varepsilon_0\varepsilon_{r_2}\frac{A}{d_2} \tag{2.35}$$

$$C_{tot} = \varepsilon_0\varepsilon_{r_{eff}}\frac{A}{d} \tag{2.36}$$

where d_1, d_2 and d are the thicknesses of the oxidized layer, reduced interior and total sample, respectively, and $\varepsilon_{r_1}, \varepsilon_{r_2}$ and $\varepsilon_{r_{eff}}$ are effective dielectric constants for the oxidized layer, reduced interior and the whole sample. A is the area of electrode. The effective dielectric constant on substitution in equation (2.33) can be obtained as follows,

$$\varepsilon_{r_{eff.}} = \frac{\varepsilon_{r_1}\varepsilon_{r_2}d}{2d_1\varepsilon_{r_2}+d_2\varepsilon_{r_1}} \qquad (2.37)$$
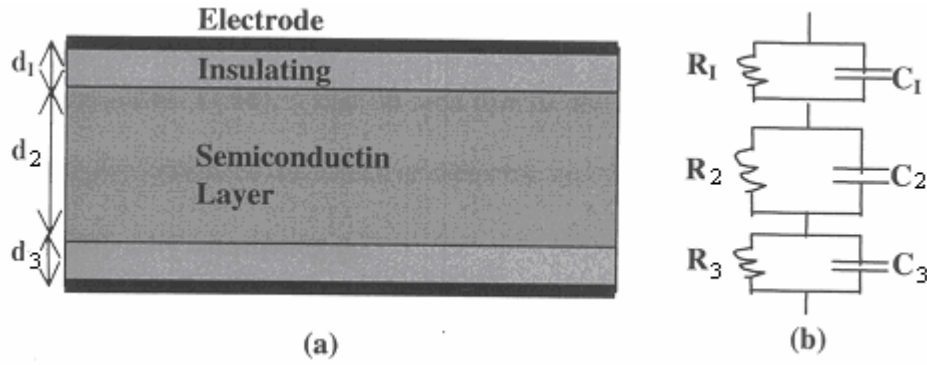
Figure 2.26 (a) Barrier layer effect (b) an equivalent circuit for (a).

From equation it can be seen that minimizing the thickness of insulating layer d_1, maximum effective dielectric constant $\varepsilon_{r_{eff.}}$ can be obtained. The structures, considered above, consisted of a conducting titanate ceramic in contact with a layer of oxidized, insulating ceramics. In reality, however, there is not a abrupt change from conducting to insulating but a diffused transition zone. The transition region in itself contain a region of grain boundary barrier layer capacitor type microstructure as shown in figure 2.27. This is as result of differential rate of oxidation and/or reduction within the grains and at their boundaries.

semiconductive | grain boundary | electrode | electrode
barrier layer | barrier
layer
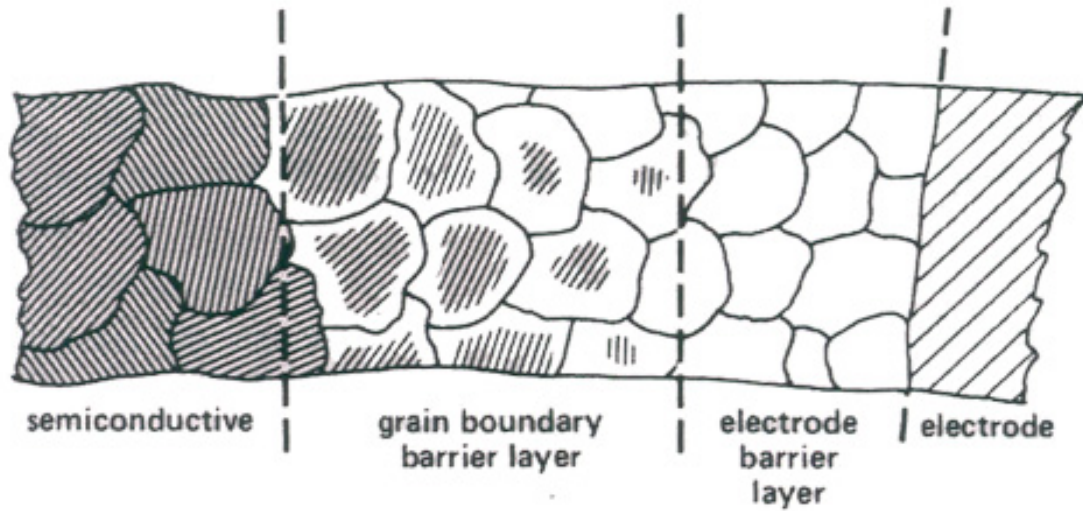
Figure 2.27: Structure of surface barrier layer.

In addition both the core-shell microstructure can be combined with macroscopic surface barrier layer capacitor to enhance the dielectric properties. Apart from having high dielectric constant, such structures have high breakdown voltage. The lower breakdown voltage, which restricts the barrier layer capacitors to low voltage application, can be thus overcome by combination of core-shell microstructure and surface barrier layer macroscopic structure. As will be discussed in next sections, the high dielectric constant and high breakdown voltage are essential in high strain application.

2.7. Internal Stress origin:

The non-uniform structures discussed above have internal stress generated in them. Following section covers the origin of internal stress

2.7.1 Microscopic stress:

Internal stress is known to be associated primarily with unit cell volume expansion which results from cubic to tetragonal phase transition. Since the grain core and grain shell are of different chemical expansion in core shell grains, on

50

cooling the grain core is in compression. The resultant internal stress does cause domain reorientation due to ferroelastic switching as well as results in high spontaneous polarization.

2.7.2 Macroscopic stress:

In addition to internal stress the surface barrier layer structures have macroscopic stress induced in them due to following reasons:

a) **Different thermal expansion coefficient:**

The layers with different expansion coefficient when pressed and sintered together will be in pre-stressed condition. This is because of difference in contraction, on cooling. The layer which contracts more will be in tensile stress and layer which contracts less will be in compression. This anisotropic stress system is observed in both functionally graded and RAINBOWS.

b) **Volume difference between reoxidized and reduced portion:**

The volume difference between the reduced and reoxidized part was studied on Mn-acceptor doped Barium titanate ceramics. The length of a ceramic bar was measured on the change from reducing to oxidizing atmospheres at 888^OC. In reducing atmosphere BT forms oxygen vacancies and conduction electrons, which gives rise to semiconductivity. Reoxidation of the same BT specimen leads to a valence change from Mn^{2+} (r=0.083nm) to Mn^{3+} (r=0.0645nm) or even Mn^{4+} (r=0.053nm). The valence change of Mn gives rise to small changes of the ionic radius and subsequently to measurable dimensional changes in the ceramic body. This can be detected by a sensitive dilatometer. Figure 2.28 shows that a rapid change in sample length occurred until equilibrium was obtained with

changing atmospheres. The original length of the sample could be regained by switching back the atmosphere. The decrease of the sample length at reoxidation is believed due to the valence change of the large Mn^{2+} ions to the smaller Mn^{3+} or Mn^{4+} ions as well to a decrease in the concentration of oxygen vacancies.[73]
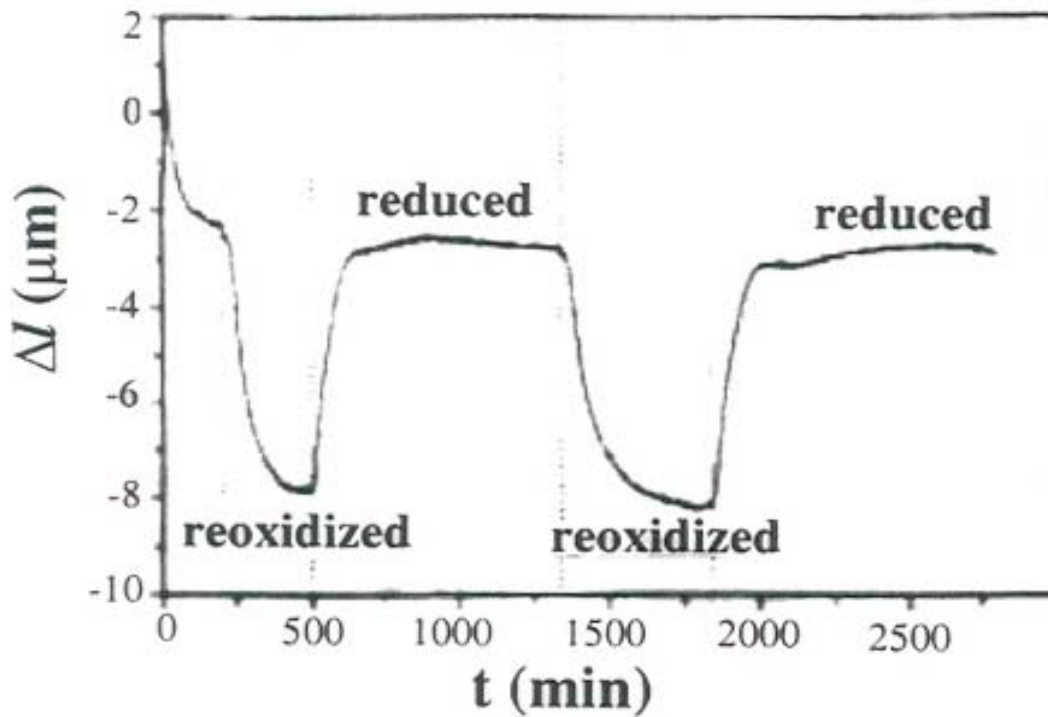
Figure 2.28: Reversible length change of a ceramic bar at reduction and oxidation atmospheres at 888°C. [72]

The mechanism for the change in internal expansions due to heating and different atmosphere is not clearly understood. However, the reduction and oxidation processes have clearly been shown to result in thermal expansion mismatch in titanate based ceramics. Consequently extra macroscopic stress will be induced anisotropically within the ceramic cross-section in addition to the internal stresses already isotropically developed by the phase transition of BT.

Rainbows consist of unreduced and reduced PZT layers, whereas surface barrier layer capacitors consist of oixidized surface layer and reduced interior

region. The contributing factors to the dimensional mismatch in rainbows are characterized as:

i)   different thermal expansions of the two layers (that of reduced was greater)

ii) the volume difference

iii) different dimensional changes at the phase transitions during cooling and

iv) the formation and diffusion of oxygen vacancies during reducing process.[73,74]

In this PZT Rainbow, an induced anisotropic stress was found through XRD measurement, indicating that the entire reduced layer is in tension and unreduced layer is in compression. Under the influence of anisotropic stresses, domain reorientation is enhanced, as shown in figure 22, due to ferroelastic switching. Here, the anisotropic stress is similar to two dimensional stress than to hydrostatic microscopic stress. It should be noted that in polycrystalline BT and PZT ceramics there are large number of random polarization directions with only locally aligned polarization and thus the ceramic exhibits isotropic bulk properties. However, when this equilibrium low energy state is disturbed under the anisotropic stress state, the material responses may no longer be isotropic, due to the combined effects of a piezoelectricity and the built-in non uniform internal stress.

Similarly BaTiO$_3$ single crystal has been used to generate a large electrostriction by coupling stress-induced and electric field induced domain switching. The maximum electrostrictive strains of 0.8 % were obtained, close to the theoretical maximum of 1.1%. Figure 2.29 illustrates the experiments carried

out in which a thin single crystal plate of (001) orientation is subjected to a constant compressive stress and variable electric field.
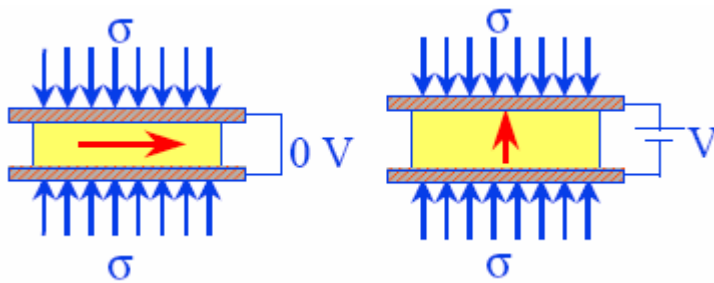
Figure 2.29: Mode of operation of an actuator based on combined electromechanical loading of a ferroelectric single crystal [75]

At room temperature $BaTiO_3$ crystal is spontaneously polarized in the <100> direction. Without applied voltage, the stresses (fixed load applied to crystal) forces the polarization to be in plane e.g., perpendicular to the thickness,[010] direction. With an increasing electric field, the polarization tends to align in the [001] direction while the stress resists it. At a certain critical voltage, the electric field overcomes the resistance by the stress and the polarization suddenly switches to [001], accompanied by 0.8% strain. As the electric field decreases, the polarization returns to in-plane, recovering the strain (Figure 2.30.)
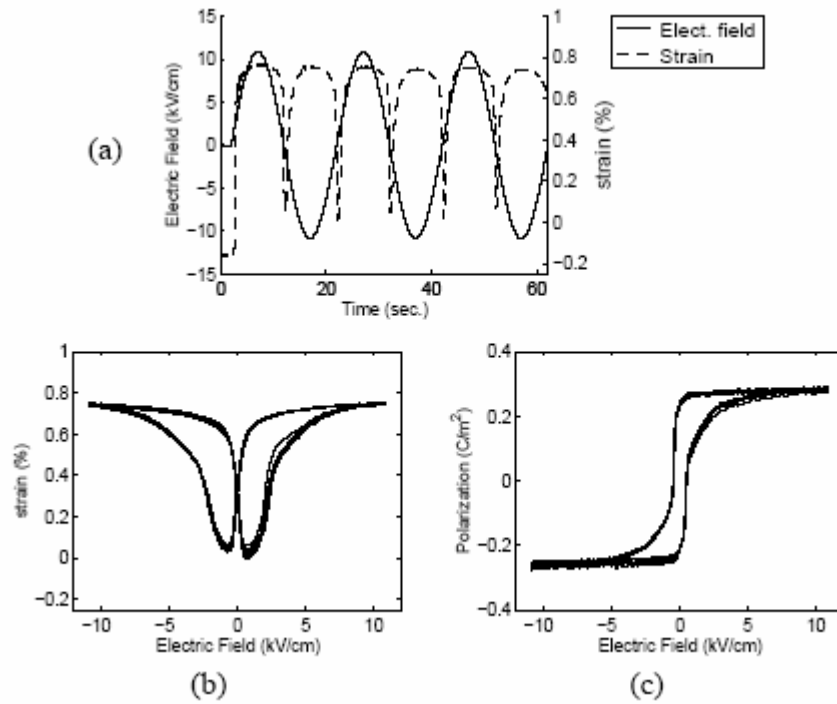
Figure 2.30: (a) Electric field and strain vs. Time (b) Strain and (c) polarization vs. electric field for a (100) oriented crystal at 1.07 MPa compressive stress.[75]

Chapter 3

Experimental

3.1. Processing of functionally graded Barium Titanate:

As a starting material, high purity $BaTiO_3$ [Ticon-HPB, TAM ceramics, Inc., Niagara Falls NY (0.987)Lot # 762] with a Ba/Ti ratio of 0.987 was used. The impurity concentration of SrO, SiO_2, Al2O3 and Fe2O3 was less than 0.1% and average particle was 1.23 μm.

As minor dopants, Nd_2O_3 and ZrO_2 were used as nitrate additives, $Nd(NO_3)_3.xH_2O$ and $ZrO(NO_3)_2.xH_2O$ [Aldrich Chemical Co., Milwaukee, WI). The nitrates were dissolved, stirred in a solvent mixture of 40 vol % de-ionized water and 60 vol % isopropanol and analyzed for oxide contents (Nd_2O_3 and ZrO_2 per millimeter solution. This was accomplished by weighing 10 mm of nitrate solution in a platinum crucible and heating slowly up to 550^OC and holding at that temperature for an hour. The remaining residue was then weighed and calculated for the oxide concentration in the nitrate solution.

In this study 0.05 to 0.3m/o of Nd_2O_3 and 2 m/o ZrO_2 was added to $BaTiO_3$. For each batch used, 100 grams of oxide mixture was prepared. The appropriate nitrate solutions were first neutralized at 7-7.5 pH using NH_4OH solution, followed by addition to the $BaTiO_3$ powder in a 250 ml jar together with 60/40 solution (40 vol % de-ionized water and 60 vol % isopropanol) and 1 wt fish oil (Werner G. smith Co., Cleveland, OH) as dispersant.

At the first ball milling, the batch containing $BaTiO_3$ and nitrate solutions was ball milled for 12 hours with stabilized zirconia media weighing 650 grams. The

second ball milling was carried out for 1.5 hours after further addition of 1 wt% of both PVA [Grade 70-05, E.I. du Pont de Nemours & Co., Inc., Wilmington, DE] and Carbowax 4000 [Union Carbide, Danbury, CT]. PVA and Carbowax function as binders that provide strength to the ceramic green body by binding the particles together.

After milling process, the slurry was spray dried using Buchi 190 Mini sprayer [Brinkman Inc., Westbury, NY] with the following settings: air flow= 675 ml/min; inlet temperature=185°C; outlet temperature=105°C; Aspirator=12. The fine powders were collected and stored in glass bottle. O.2 grams each of 0.05 m/o Nd 2 m/o of Zr, 0.15 m/o Nd 2 m/o of Zr and 0.3 m/o Nd 2 m/o of Zr powders were weighed and uniaxially pressed in three stages into disc shaped pellets for the characterization. The green pellets had a diameter ~10.25 mm and a thickness ~ 1.2 mm. These are then sintered at 1300°C for 90 minutes.

3.2. Density Measurement

The as-sintered pellets were polished with 600 grit and 1200 grit SiC. Density of sample was determined by measuring the geometry. Weight, W, and dimensions like diameter, d, and thickness, t were measured and thus geometry density, ρ_g was calculated by using following equation

$$\rho_g = \frac{4W}{\pi d^2 t}$$ (3.1)

Theoretical density for $BaTiO_3$ with Nd_2O_3 and ZrO_2 additives were calculated using the mixing rule

3.3. Dielectric Property Measurement

Pellets used for geometric density measurements had the smooth surface for electrodes to be put on them. The electrodes were then applied on samples by evaporation sputtering of aluminum. This process was repeated to achieve the surface resistance less than 1.

The capacitance and loss tangent were measured as a function of both temperature and frequency. For the temperature dependence, the measurements were performed with an LCZ meter [4276 A LCZ Meter, Hewlett-Packard, Palo, Alto, CA] connected to the computer through GPIB. The schematic of the sample holder and connection is illustrated in figure 3.1. Samples were then placed in the shielded specimen chamber and the spacer was used between the tip of the probe and sample surface to produce the even electric field across the samples. The automatic measurement was followed at slow heating rate of 2 to 3°C/min.

Measurements for frequency dependence of the capacitance and loss tangent were done at room temperature. The samples were placed in a shielded, custom designed sample holder, which is shown in figure 3.2. The sample holder was connected shielded leads to an automatic impedence/gain phase analyzer [4194 A Impedence/Gain Analyzer] phase Analyzer, Hewlett Packard, Palo Alto, CA] having the frequency range from 100Hz to 40 MHz and output voltage of 8 Vrms. The capacitance and impedence in the measurement circuit were minimized by carrying out the "zero open and zero short" compensation of the

sample and leads. The measurements were controlled by the computer and the resulting data stored for further analysis and plotting.
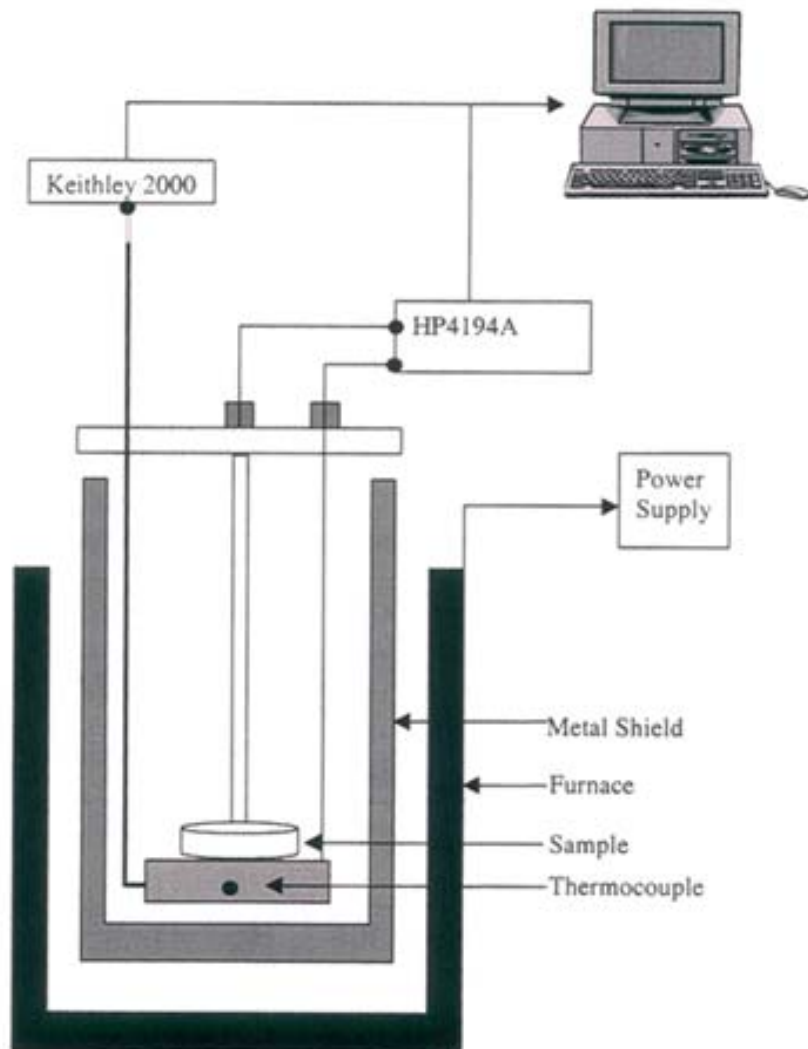
Figure 3.1: Set-up to measure the temperature dependence of dielectric properties.
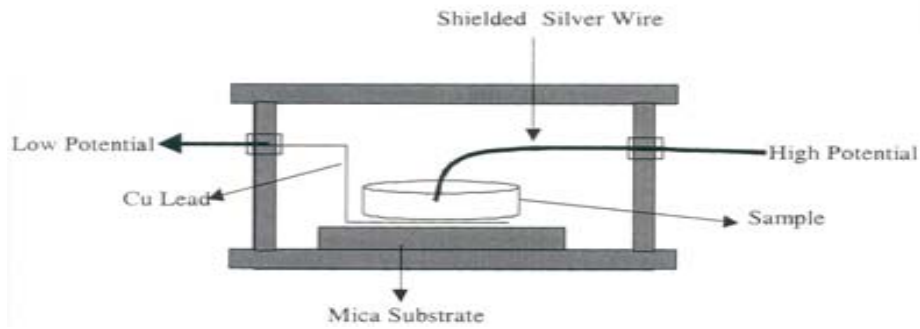
Figure 3.2 Sample holder to measure the frequency dependence of dielectric properties.

3.4. Strain measurement:

An experimental set-up to measure the electric field induced strain is shown in figure 3.3. The transformer used as a displacement sensor is LVDT (linear variable differential transformer) manufactured by Lucas Schaervitz Co. (Model MP-2000). As depicted in the figure, a specimen is placed in the plastic container which is filled with silicon oil for the insulation purpose. A voltage was applied across the sample electrodes through the bottom plate of the container and the LVDT movable rod. The applied field was changed gradually with variable to obtain a complete strain loop.
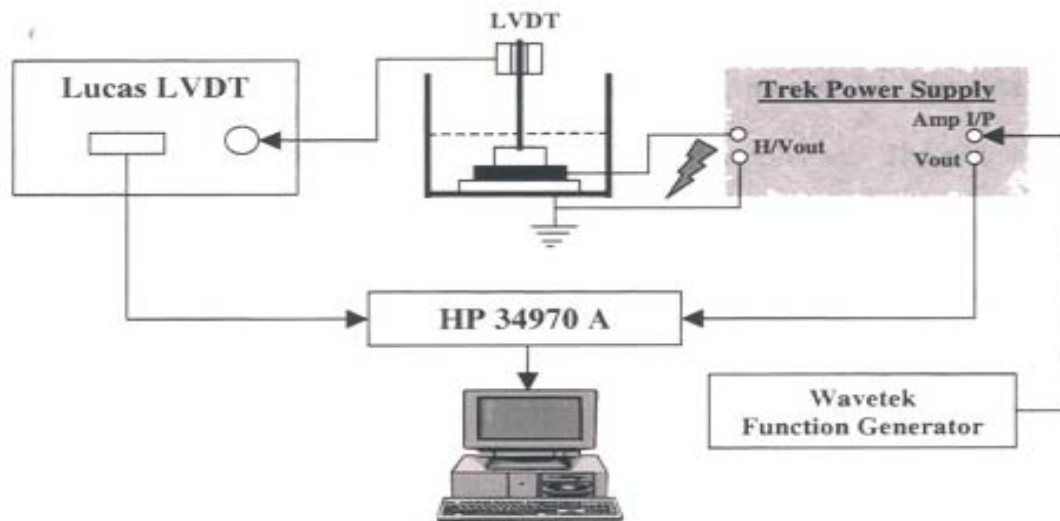
Figure 3.3: Strain Measurement Set-Up.

Chapter 4

Equations Derived and Discussion

4.1 Mathematics of relation between dielectric constant and spontaneous polarization to strain

Our investigation of doped barium titanate had revealed that to obtain high strain it was important to maximize dielectric constant and spontaneous polarization change, on application of electric field. Therefore following equations were derived to relate dielectric constant and spontaneous polarization to strain:

Free charge is permitted to appear only on part of the surface of a simulated ceramic. For the ceramic with a volume V, conservation of charge requires [76]

$$\partial D_i / \partial x_i = 0 \tag{4.1}$$

where D is the electric displacement and x is the position vector. Continuity of charge at crystallite boundaries requires that [76]

$$n_i [| D_i |] = 0 \tag{4.2}$$

where n is the unit normal to the surface and the symbol [| |]denotes a jump in the quantity contained within the surface. Without body force, mechanical equilibrium requires

$$\partial \sigma_i / \partial x_i = 0 \tag{4.3}$$

where σ is the mechanical stress; continuity of stress at crystallite boundaries requires that [76,77]

$$n_i [| \sigma_i |] = 0 \tag{4.4}$$

The elasticity law for a given crystallite is [78]

$$\sigma_{ij} = C_{ijkl}e_{kl} + \gamma_{kij}E_k \tag{4.5}$$

where C is the elastic tensor, e the strain tensor defined by

$$e_{ij} = \partial u_i / \partial x_i + \partial u_j / \partial x_j / 2 \tag{4.6}$$

where u is the displacement vector; γ_{ijk} is the converse piezoelectric coefficient tensor defined by

$$\gamma_{ijk} = d_{ilm}C_{lmjk} \tag{4.7}$$

where d is the direct piezoelectric coefficient tensor giving the linear part of the strain e under an applied field E and the linear part of the electric displacement D under an applied stress σ.The constitutive law gives the electric displacement D.[78]

$$D_i = \gamma_{ijk}e_{jk} + \varepsilon_0\varepsilon_{ij}E_j + P_i^s \tag{4.8}$$

where P^s is the spontaneous polarization of the crystallite, ε_{ij} is dielectric constant, and E the electric field vector

$$E_i = \partial\phi_i / \partial x_i \tag{4.9}$$

where ϕ is the potential

The elastic energy is given by

$$\frac{1}{2}\sigma_{ij}e_{ij} = \frac{1}{2}\left(C_{ijkl}e_{kl}e_{ij} + \gamma_{kij}E_k e_{ij}\right) \tag{4.10}$$

The Dielectric and piezoelectric energy is given by

$$\frac{1}{2}E_i(D_i - P_i^s)$$
$$= \frac{1}{2}\left[(\gamma_{ijk}e_{jk}E_i + \varepsilon_0\varepsilon_{ij}E_jE_i + E_iP_i^s) - E_iP_i^s\right] \tag{4.11}$$

The elastic energy and dielectric and piezoelectric energy are equal because mechanical energy is direct manifestation of electric energy applied. Therefore, considering the bulk properties, after applying the electric field, ΔE there would be a state change. The spontaneous polarization of the switched crystallite changes from its old value P^S to a new value $P^S + \Delta P^S$. Due to the applied electric field and change of the spontaneous polarization strain becomes Δe. When the electric field is applied in 3-direction and strain is measured in that direction, virtual work provides,

$$[\Delta e_3]^2 C_{33} = \varepsilon_0 \varepsilon_{33}[\Delta E_3]^2 + \Delta E_3 \Delta P_3^s \qquad (4.12)$$

From equation (4.12) it can be concluded that the increase in dielectric constant and increase in change of spontaneous polarization will increase the strain. Dielectric constant of $BaTiO_3$ can be increased by doping it with ZrO_2 and Nd_2O_3 (due to core shell grains in combination with GBBLC) and by surface barrier layer effect. The method of producing the surface barrier layer structure is by incorporating the conducting layer between the two insulting layers. The conducting layer is selected from resistivity minima which is generally 0.1 to 0.15 mole % of Nd_2O_3 content.

On introduction conducting layer between two insulators, there would be differential "macroscopic" stress state developed in the structure. This is because; the gradient in Nd^{3+} will induce the unit cell volume difference in the structure over the thickness direction. If the structure is asymmetric (i.e. the two insulating layers are of different compositions, hence the functionally graded

structure) the difference in thermal expansion mismatch will contribute to characteristic dome shape as in RAINBOW.

The differential stress state will lead to preferred domain orientation and hence the high spontaneous polarization change on application of high field. This would additionally lead to high strain along with high dielectric constant term.

When the three layers with different dielectric constants are pressed together and sintered together, the dielectric constant of this structure (capacitors in series as in figure (4.1) is given by,

$$\varepsilon_{reff.} = \frac{\varepsilon_1\varepsilon_2\varepsilon_3(d_1 + d_2 + d_3)}{d_1\varepsilon_2\varepsilon_3 + d_2\varepsilon_1\varepsilon_3 + d_3\varepsilon_1\varepsilon_2}$$

(4.13)

$\varepsilon_{reff.}$ is the effective dielectric constant,

$\varepsilon_1, \varepsilon_2, \varepsilon_3$ are the permittivities of different layers and

d_1, d_2, d_3 are the thickness of different layers.
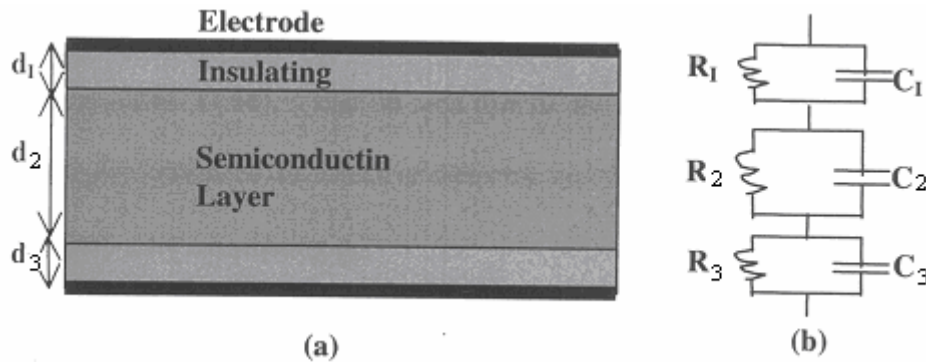
Figure 4.1 (a) Barrier layer effect (b) an equivalent circuit for (a).

It can be seen with equation (4.13) that if the permittivity is increased for one layer, then the effective permittivity is increased. This can be accomplished by introducing the semiconducting layer in between the insulating layer. The space

charge polarization of the middle layer will increase the dielectric constant due to barrier layer effect.

In the ferroelectric material, the spontaneous polarization is nonzero and the polarization of the material, P, under the small applied field is given by:

$$P = P^s + \varepsilon_0 \varepsilon_{reff.} \Delta E \qquad (4.14)$$

so that displacement x of material with electrostrictive coefficient Q on application of electric field ΔE is given by [39]

$$x = Q(P^s + \varepsilon_0 \varepsilon_{reff.} \Delta E)^2 = Q(P^s)^2 + 2Q\varepsilon_0 \varepsilon_{reff.} P^s \Delta E + Q\varepsilon_0^2 \varepsilon_{reff}^2 (\Delta E)^2 \qquad (4.15)$$

The spontaneous strain is given by,

$$x_s = Q(P^s)^2 \qquad (4.16)$$

The electrostrictive strain is given by,

$$x_e = Q\varepsilon_0^2 \varepsilon_{reff}^2 (\Delta E)^2 \qquad (4.17)$$

Therefore piezoelectric coefficient d may be expressed as,

$$d = 2\varepsilon_0 \varepsilon_{reff.} QP^s \qquad (4.18)$$

where d = piezoelectric coefficient,

ε_0 = permittivity of free space,

$\varepsilon_{reff.}$ = effective dielectric constant of functionally graded structure,

Q = electrostrictive coefficient,

P^s = spontaneous polarization.

Thus from the equation (4.18) (which is from literature) again, it can be inferred that raising the dielectric constant and the spontaneous polarization term, would raise the strain due to increase in piezoelectric coefficient.

4.2. Calculation for dome-shaped asymmetrical structures:

The strain data was obtained by LVDT in which probes were placed on top and bottom of the sample. Therefore strain obtained was along thickness direction. To find the effective piezoelectric coefficient (d_{31}) it was necessary to find strain along direction perpendicular to thickness direction. Following equations were derived to meet this requirement.
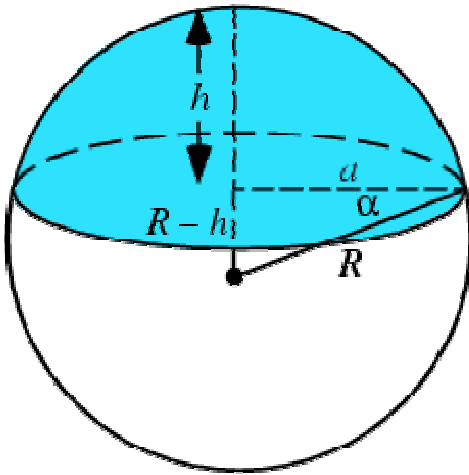
Figure 4.2 Illustration of spherical cap.

The volume of spherical cap is given by

$$V_{cap} = \frac{1}{6}\pi h(a^2 + h^2)$$ (4.19)

where, a = radius of a cap,

h= height of a cap.
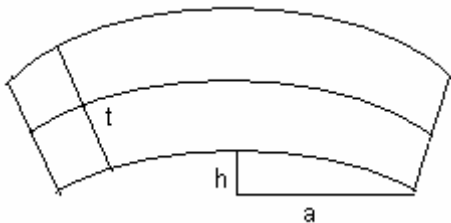
Figure 4.3a: Dome Shaped asymmetric sample without application of electric field

Volume of dome = Volume of outer spherical cap- Volume of inner spherical cap

$$V_{dome} = \frac{1}{6}\pi(h+t)[(a+t)^2 + (h+t)^2] - \frac{1}{6}\pi h(a^2 + h^2) \qquad (4.20)$$

On application of field strain is induced. It will result into more flattening out of dome structure. The new dimensions of the dome shape are as indicated in a figure below
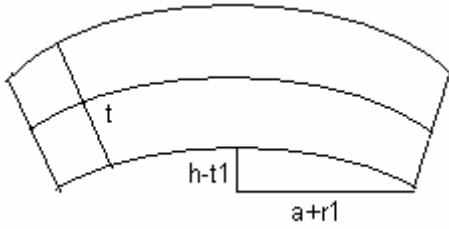
Figure 4.3b: Dome Shaped asymmetric sample on application of electric field

$$V_{dome.app.} = \frac{1}{6}\pi(h+t-t_1)[(a+r_1+t)^2 + (h+t-t_1)^2] - \frac{1}{6}\pi(h-t_1)[(a+r_1)^2 + (h-t_1)^2]$$

$$(4.21)$$

$$V_{dome} = V_{dome.app.} \qquad (4.22)$$

Solving this equation we get r_1 and therefore strain is r_1/a

From equation below d_{31} is obtained

$$\Delta e_{31} = d_{31}\Delta E_3 \qquad (4.23)$$

Chapter 5

Results and Discussion

5.1 Effect of combined doping of ZrO_2 and Nd_2O_3 on $BaTiO_3$

Addition of ZrO_2 and Nd_2O_3 in $BaTiO_3$ lead to core-shell grains (figure 5.1) with core under compressive stress. The relatively low densities observed in single doped $BaTiO_3$ with high Nd_2O_3 are significantly improved with combined doping of zirconia. More than 93% theoretical densities are obtained. Nd_2O_3 single addition exhibit significant decrease in grain size with uniform distribution of fine grains. There is also a gradual structure change from tetragonal to pseudocubic as a function of the combined dopant concentrations. The dielectric constant of this doped BaTiO3 is also high; of the order of 20,000 to 35,000.

The induced stress in the core enhances the strain. This we will term as "microscopic stress" effect
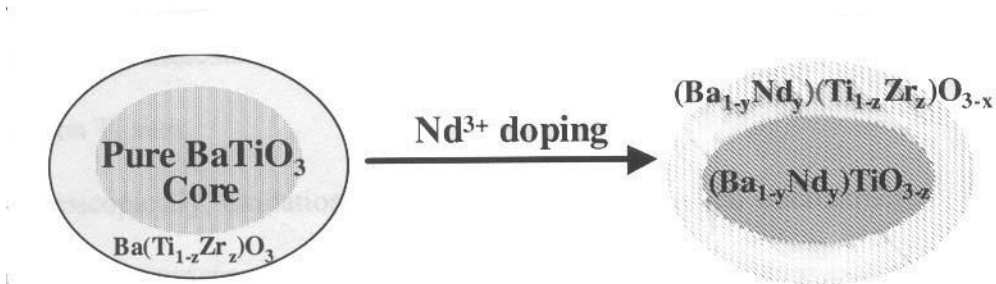
Figure 5.1: Effect of doping by donor Nd_2O_3 on ZrO_2 modified core-shell $BaTiO_3$. [21]

5.2 Data Used:

Data collected by myself and fellow group members was used for modeling as shown on next page. Both dielectric constant and strain data was used:
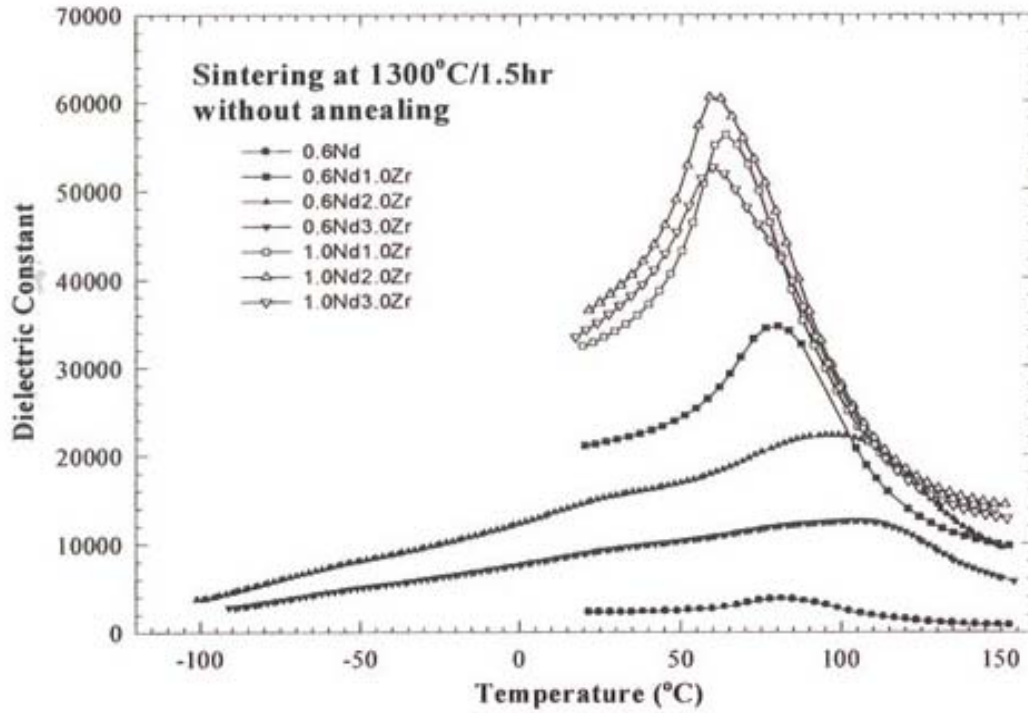
Figure 5.2: Temperature dependence of Dielectric Constant (at 1 kHz) for (1.0-3m/o) ZrO_2 and (0.6 and 1.0 m/o Nd_2O_3 doped $BaTiO_3$ ceramics (sintered 1300°C for 1.5hrs)
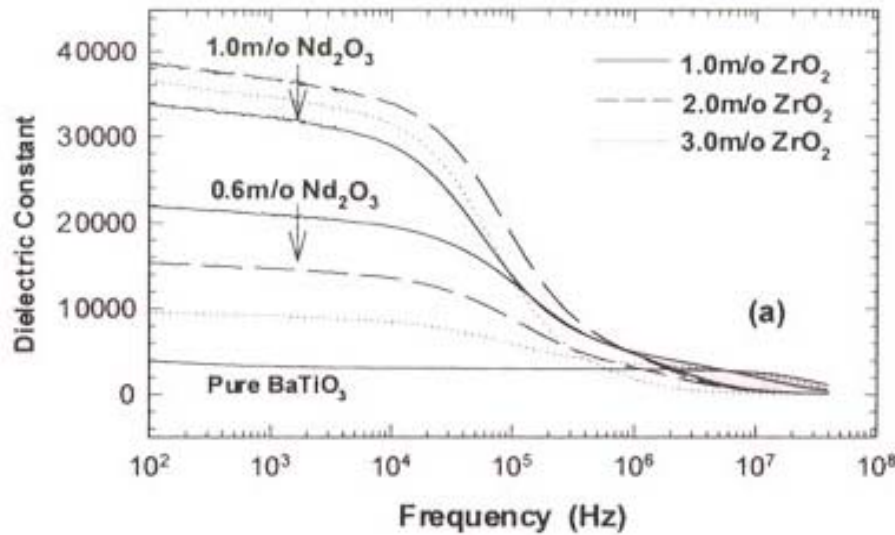
Figure 5.3: Frequency dependence of Dielectric constant Nd_2O_3 and ZrO_2 doped $BaTiO_3$.
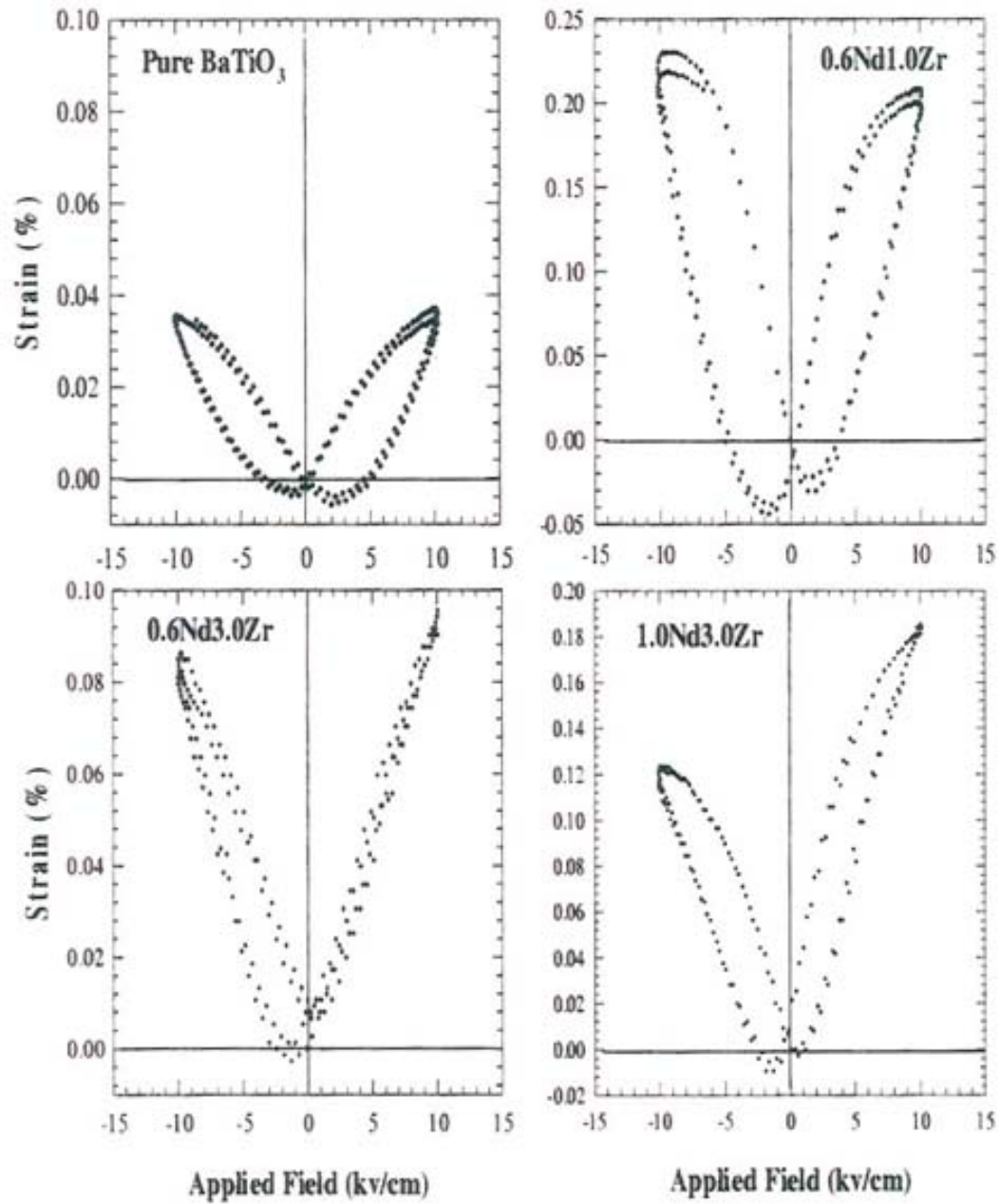
Figure 5.4: Strain data for modified barium titanate sintered at 1320°C/1.5 hr.
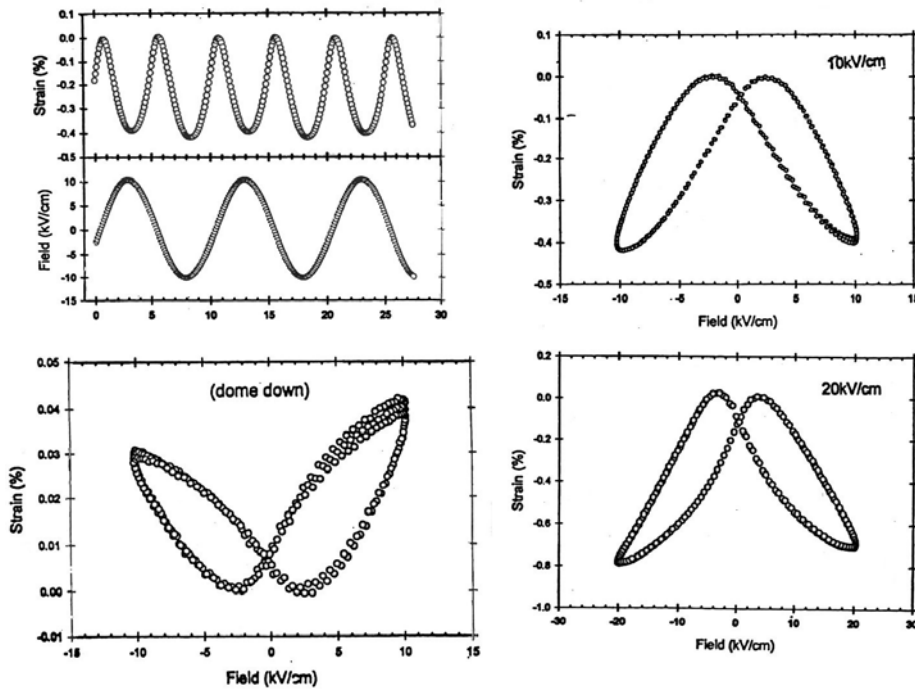
Figure 5.5: Strain data for functionally graded barium titanate.

From figure 5.2 and 5.3 it is clear that addition of ZrO_2 and Nd_2O_3 to $BaTiO_3$ significantly increase the dielectric constant by formation of core-shell grain microstructure. As discussed this leads to increase in strain, as indicated in figure 5.4. Figure 5.5 shows strain characteristic for dome shaped functionally graded $BaTiO_3$. The composition for dome shape is 0.05 m/o Nd for first layer, 0.15 m/o Nd for second layer and 0.3 m/o Nd for third layer. The ZrO_2 content is 2 wt % for all the three layers.

5.3 Calculations for spontaneous polarization change and piezoelectric coefficient

For pure Barium Titanate

Basic Data

Piezoelectric Coefficient, $d_{33} = 320 \times 10^{-12}$ C/N

Electric Field, ΔE_3 = 10kV/cm=10^6 V/m

Dielectric Constant, ε_{33}=800

Young's Modulus, Y=67GPa=67 x 10^9 N/m^2

Total strain in 3-direction, Δe_T =?

Piezoelectric Strain in 3-direction, Δe_p =?

First we calculate piezoelectric strain,

$\Delta e_p = d_{33}\Delta E_3$

$\quad$ = 320x10^{-12} x 10^6

$\quad$ = 3.2 x 10^{-4}

Electrostrictive strain= total strain-piezoelectric strain

$$= 0.512 \text{ x } 10^{-4}$$

The basic equation we have derived is (equation 4.12),

$\quad \Delta e_T Y \Delta e_T = [\Delta E_3 \varepsilon_{33} \varepsilon_0 \Delta E_3 + \Delta P^s \Delta E_3]$

(3.712 x 10^{-4})^2 x 67x10^9= [(10^6)^2 x 800 x 8.85 x 10^{-12} + ΔP^s x 10^6

$\quad\quad \Delta P^s$ = 0.00215 C/m^2

Thus this is 10^{-3} term. The actual spontaneous strain of pure barium is 0.21 C/m^2. Thus change is just about 1% on application of field. This happens due to domain reorientation. Thus we can conclude that the domain reorientation effect is marginal.

Strain calculation for 0.6 Nd 1Zr

Δe_T = 2.3 x 10^{-3}

$\Delta e_p = \Delta e_T - \Delta e_{annealing}$

= 2.0×10^{-3}

ε_{33} = 20,000

Basic equation is

$$\Delta e_T Y \Delta e_T = [\Delta E_3 \varepsilon_{33} \varepsilon_0 \Delta E_3 + \Delta P^s \Delta E_3]$$

$(2.3 \times 10^{-3})^2 \times 67 \times 10^9 = [(10^6)^2 \times 8.85 \times 10^{-12} \times 20000] + \Delta P^s \times 10^6$

ΔP^s **= 0.177 C/m^2**

This is much higher than barium titanate. Two order of a magnitude higher. This is because of domain reorientation. Additionally the weightage of term is about 50%. Thus there is sizable effect of domain reorientation on strain.

$$\Delta e_p = d_{33} \Delta E_3$$

d_{33} = 200×10^{-11} C/m^2

Thus we observe increase of one order of magnitude in d_{33} than pure barium titanate.

Calculation for dome-shaped asymmetrical structures:

The volume of spherical cap is given by (refer equation 4.19),

$$V_{cap} = \frac{1}{6}\pi h(a^2 + h^2)$$

From equation 4.20,

$$V_{dome} = \frac{1}{6}\pi(h+t)[(a+t)^2 + (h+t)^2] - \frac{1}{6}\pi h(a^2 + h^2)$$

For a=10 mm h=0.5 mm t = 1mm

$$V_{dome} = \frac{1}{6}\pi(0.5+1)[(10+1)^2 + (0.5+1)^2] - \frac{1}{6}\pi h(10^2 + 0.5^2)$$

$$V_{dome} = \frac{1}{6}\pi(134.75)\,\mathrm{mm}^3$$

On application of field strain is 2 %.Substituting in equation 4.21 we get,

$$V_{dome.app.} = \frac{1}{6}\pi(h+t-t_1)[(a+r_1+t)^2+(h+t-t_1)^2] - \frac{1}{6}\pi(h-t_1)[(a+r_1)^2+(h-t_1)^2]$$

$$= \frac{1}{6}\pi\{(1.49)[(11+r_1)^2+(1.49)^2]-(0.49)[(10+r_1)^2+(0.49)^2]\}$$

$$= \frac{1}{6}\pi\{134.48+22.8r_1+r_1^{\,2}\}mm^3$$

$$V_{dome} = V_{dome.app.}$$

$$(134.48+22.8r_1+r_1^{\,2}) = 134.75$$

$$r_1^{\,2}+22.98r_1-0.27=0$$

Solving this equation we get

r_1 = 0.0196 mm

therefore strain is 0.0196/a=0.00196

Δe_{31} =0.00196

$$\Delta e_{31}Y\Delta e_{31} = (\Delta E_3 d_{31}Y\Delta e_{31})$$

1.96 x 10^{-3} = (10^6 x d_{31})

d_{31} = 1.96 x 10^{-11} C/m^2

Thus we see that even for lower value of effective d$_{31}$ the strain is quite high because of dome shape.

5.4 Mechanisms of developing bending deformation in functionally graded materials:

Finite element analysis for simplified model of functionally graded piezoelectric structures revealed that the in-plane strain for different layers was

different. When the distribution of in-plane strain is linear in the thickness direction, a natural bending deformation can be produced without internal stress. The layer to generate high strain has large piezoelectric constants but small dielectric constants. In contrast, the low-strain layer has small piezoelectric constants but large dielectric constants. The stress distribution in the actuator depends on the thickness ratio of the layers. A four-layer structure as shown in figure 5.6 (a) is used to illustrate this point. The intermediate layers have intermediate values of material properties. Due to the gradation of material properties, the layers will generate a graded distribution of in-plane strain as shown in figure 5.6(b) when they are considered separately. Since all the layers are integrated in a single element, a bending deformation is generated as shown in figure 5.6(c) with relatively small internal stress.

(a)

(b)

(c)
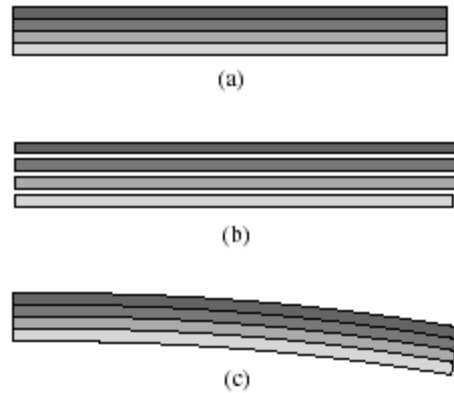
Figure 5.6: Mechanism of bending deflection. [79]

Since all the layers are integrated into a single element and no internal electrodes are inserted between the layers, the component of electric displacement in the thickness direction, D_3, is the same in all the layers. The electric field in the i th layer, $E_{3,i}$, can be written as [20]

$E_{3,\,i} = D_3/\varepsilon_{33,i}$ (59)

where $\varepsilon_{33,i}$ is permittivity.

Thus the voltage drop across would be more on layer with low dielectric constant and less across the layer with high dielectric constant. This would avoid the voltage loss in layer with low piezoelectric constant.

5.5 Numerical Characterization of functionally graded layer and results for different compositional variation (according to power law) :

The material comprises a piezoelectric layers, and a graded layer (figure 5.7). The material may be stacked symmetrically or asymmetrically with respect to the reference plane. The variation of material properties over FGM thickness is defined as

$$P(x_3) = P_1 + \Delta P N(x_3))$$ (5.1)

where, $\Delta P = (P_1 - P_2)$, P_1 and P_2 are the material properties of the first ferroelectric and the second ferroelectric layer respectively and the function $N(x_3)$ is the compositional variation of the material in the graded layer.
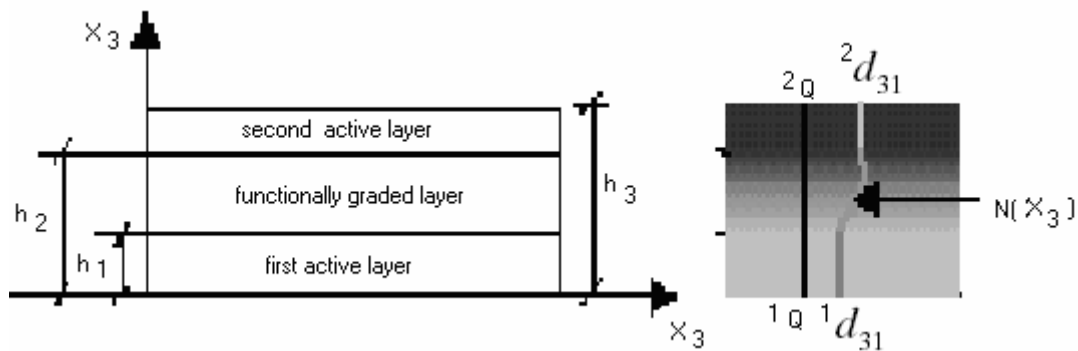
Figure 5.7: Layer structure and property gradation of an electro-elastically graded material.

The augmented linear constitutive relations for electroelastically graded materials are defined as [80]

$$\sigma_{ij} = Q_{ijkl}(\varepsilon_{kl} - d_{klm}E_m - \bar{d}_{klm}E_m\Delta T - \alpha_{ij}\Delta T) \tag{5.2}$$

$$D_m = d_{kji}Q_{ijkl}\varepsilon_{kl} - \bar{d}_{kji}Q_{ijkl}\varepsilon_{kl}\Delta T - \xi_{km}E_m - \bar{\xi}_{km}E_m\Delta T - p_m\Delta T) \tag{5.3}$$

where σ_{ij} is the second-order stress tensor, Q_{ijkl} is the fourth order stiffness tensor as a function of the thickness of material,(x_3) ε_{kl} is the second-order strain tensor, d_{klm} is the third-order piezoelectric strain tensor as a function of x_3,

D_m is the dielectric displacement vector, ξ_{km} is the second-order permittivity tensor as a function of x_3, E_m is the electrical field vector, p_m is the pyroelectric coefficient vector, and ΔT is the change in temperature from the reference state (that is, a state free of thermal residual stress).

Equations (5.2) and (5.3) represent the modified converse and the direct piezoelectric effects to include the temperature dependence of piezoelectric properties through terms $\bar{d}_{klm}$ and $\bar{\xi}_{km}$. These properties have been shown to be relatively independent of the electric field level. For a structure with a length that is large compared to its width and thickness, the Euler–Bernoulli theory can be used for the solutions at all locations away from the edges. Further, if the voltage is applied across the thickness, then the electrical field is generated only in the x_3-direction and is denoted by E_3. We also assume that a uniform temperature difference ΔT is applied over the material thickness only. For such a case, equation (5.2) reduces to

$$\sigma_1 = Q_{11}[\varepsilon_1 - (d_{31} - \bar{d}_{31}\Delta T)E_3 - \alpha\,\Delta T] \tag{5.4}$$

where σ_1, ε_1 and Q_{11} are the stress, strain and elastic modulus, d_{31} and $\bar{d}_{31}$ are the piezoelectric strain coefficients in the x_1-direction, while the electric field is in the x_3-direction and α is the coefficient of thermal expansion. Similarly, the direct piezoelectric equation is simplified to

$$D_3 = [Q_{11}(d_{31}\varepsilon_1 - \bar{d}_{31}\varepsilon_1\Delta T) - (\xi_{33} - \bar{\xi}_{33}\Delta T)E_3 - p_3\Delta T] \tag{5.5}$$

The strain at any point (ε_1) can be expressed in terms of strain at the reference plane as follows:

$$\varepsilon_1 = \varepsilon_0 - kx_3 \tag{5.6}$$

where ε_0 is the in-plane strain and k is the curvature.

Noting that the piezoelectric properties now include temperature effects and using the variable definitions from figure 5.7, the constitutive relations in equations (5.4) and (5.5) can be elaborated as

$$\sigma_1 = [^1Q_{11} + \Delta Q N(x_3)\gamma][\varepsilon_0 - kx_3 - (^1d'_{31} - \Delta d'_{31}\bar{N}(x_3)\gamma)E_3 - \alpha^1 + \Delta\alpha N(x_3)\gamma\Delta T] \tag{5.7}$$

and

$$D_3 = [^1Q_{11} + \Delta Q N(x_3)\gamma](^1d'_{31} - \Delta d'_{31}\bar{N}(x_3)\gamma)\times(\varepsilon_0 - kx_3) - [^1\xi'_{33} - \Delta\xi'_{33}N(x_3)\gamma]E_3 - p_3\Delta T] \tag{5.8}$$

where $^1Q_{11}$ and $^2Q_{11}$ are the elastic moduli, $^1d_{31}$ and $^2d_{31}$ are the piezoelectric strain coefficients, and $^1\xi_{33}$ and $^2\xi_{33}$ are the permittivity coefficients of the first and the second active materials respectively. The prime indicates that the electrical

properties are temperature dependent. The mismatches are given as

$\Delta Q = {}^2Q_{11} - {}^1Q_{11}, \Delta d_{31} = {}^2d_{31} - {}^1d_{31}$, $\Delta \xi_{33} = {}^2\xi_{33} - {}^1\xi_{33}$ and $\Delta \alpha = {}^2\alpha - {}^1\alpha$. The parameter γ is defined as

$$\gamma = \begin{cases} 0 & 0 \le |x_3| \le |h_1| \\ 1 & |h_1| \le |x_3| \le |h_2|, |h_2| \le |x_3| \le |h_3| \end{cases} \tag{5.9}$$

where $| \cdot |$ represents the magnitude of the ordinate.

Using the converse piezoelectric effect, the force and bending moment equilibrium equations can be obtained from

the following expressions:

$$\int_0^{h_3} \sigma_1(x_3) dx_3 = 0 \qquad \int_0^{h_3} x_3 \sigma_1(x_3) dx_3 = 0 \tag{5.10}$$

Integrating equation (5.10), the strain components ε_0 and k are given as follows:

$$\boldsymbol{K}\varepsilon + \boldsymbol{B} = 0 \tag{5.11}$$

Where $\boldsymbol{K}$ is a 2×2matrix of rigidity coefficients, $\varepsilon_1 = (\varepsilon_0 - k)^{\mathrm{T}}$ is the vector of strains, and $\boldsymbol{B} = (b_1 b_2)^{\mathrm{T}}$ is the vector of body forces developed due to applied electrical and thermal fields.

The terms in $\boldsymbol{K}$ and $\boldsymbol{B}$ are defined as

$$k_{11} = \sum_{i=1}^{m} [{}^1Q_{11}h_1 + {}^1Q_{11}(h_2 - h_1) + \Delta Q I_1 + {}^2Q_{11}(h_3 - h_2)] \tag{5.12}$$

$$k_{12} = k_{21} = \sum_{i=1}^{m} \left[\frac{{}^1Q_{11}h_1^2}{2} + \frac{{}^1Q_{11}(h_2^2 - h_1^2)}{2} + \Delta Q I_2 + \frac{{}^2Q_{11}(h_3^2 - h_2^2)}{2} \right] \tag{5.13}$$

$$k_{22} = \sum_{i=1}^{m} \left[\frac{{}^1Q_{11}h_1^3}{3} + \frac{{}^1Q_{11}(h_2^3 - h_1^3)}{3} + \Delta Q I_5 + \frac{{}^2Q_{11}(h_3^3 - h_2^3)}{3} \right] \tag{5.14}$$

$$b_1 = \sum_{i=1}^{m} \begin{bmatrix} {}^1Q_{11}[E_3({}^1d'_{31}h_1 + {}^1d'_{31}(h_2 - h_1) + \Delta d'_{31}I_1 + \Delta T({}^1\alpha h_1 + {}^1\alpha(h_2 - h_1) + \Delta \alpha I_1)] \\ + \Delta Q[E_3({}^1d'_{31}I_1 + \Delta d'_{31}I_3) + \Delta T({}^1\alpha I_1 + \Delta \alpha I_3)] \\ + {}^2Q_{11}[{}^2d'_{31}E_3(h_3 - h_2) + {}^2\alpha \Delta T(h_3 - h_2)]] \end{bmatrix} \tag{5.15}$$

$$b_2 = \sum_{i=1}^{m} \begin{bmatrix} \dfrac{{}^1Q_{11}}{2}[E_3({}^1d'_{31}h_1^2 + 2\Delta d'_{31}I_4 + \Delta T({}^1\alpha h_1^2 + 2\Delta \alpha I_4)] \\ + \Delta Q[E_3({}^1d'_{31}I_4 + \Delta d'_{31}I_6) + \Delta T({}^1\alpha I_4 + \Delta \alpha I_6)] \\ + \dfrac{{}^2Q_{11}}{2}[{}^2d'_{31}E_3(h_3^2 - h_2^2) + {}^2\alpha \Delta T(h_{33}^2 - h_2^2)]] \end{bmatrix} \tag{5.16}$$

The integral terms (I_1–I_6) in equations (5.12)–(5.16) depend on the compositional gradation.

For the direct piezoelectric effect, using Gauss' law for electrodes in short-circuit, the induced charge (q) due to applied strain is given as

$$q = \iint_A D_3 dA \tag{5.17}$$

where the electric displacement is

$$D_3 = \int_{x_3} D_3(x_3)dx_3 \tag{5.18}$$

The capacitance of the material is

$$C = \frac{1}{h}\int_A \left(\int_{x_3} ({}^1\xi'_{33} - \Delta\xi'_{33}N(x_3)\gamma)dx_3 \right) dA \tag{5.19}$$

where h is the distance between the two electrode surfaces and A is the plan area of electrodes common to both faces of the material. The induced voltage (V) is

$$V = \frac{q}{c} \tag{5.20}$$

Compositional variations

In this work the power law function (figure 5.8) is considered to account for gradation. It is given by

$$N(x_3) = \left(\frac{x_3 - h_1}{h_2 - h_1} \right)^n$$

(5.21)
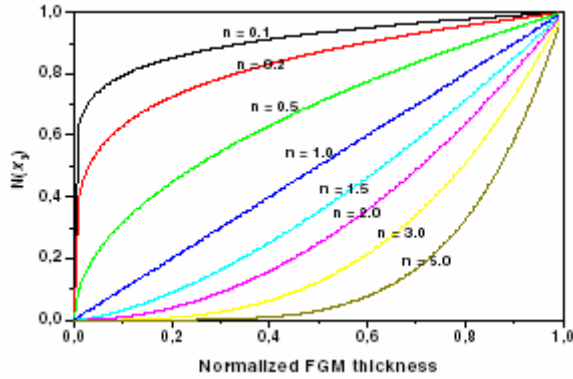
Figure 5.8: Power-law variation of electro-elastic properties in the FG layer.[80]

As the gradation function in equation (5.21) is bounded by the parameter γ defined in equation (5.9), we have

$$N(x_3) = \begin{cases} 0 & @ \ x_3 = h_1 \quad and \quad -h_1 \\ \\ 1 & @ \ x_3 = h_2 \quad and \quad -h_2 \end{cases}$$

(5.22)

The integral terms $(I_1 - I_6)$ in equations (5.12)–(5.16) for the power-law-type gradation are obtained explicitly and are given as follows:

$$I_1 = \int_{h_1}^{h_2} N(x_3)dx_3 = \frac{1}{(h_2 - h_1)^n}\left[\frac{(h_2 - h_1)^{n+1}}{n+1}\right]$$

(5.23)

$$I_2 = I_4 = \int_{h_1}^{h_2} N(x_3)x_3 dx_3 = \frac{1}{(h_2 - h_1)^n}\left[\frac{(h_2 - h_1)^{n+2}}{n+2} - \frac{h_1(h_2 - h_1)^{n+1}}{n+1}\right]$$

(5.24)

$$I_3 = \int_{h_1}^{h_2} (N(x_3))^2 dx_3 = \frac{1}{(h_2 - h_1)^{2n}}\left[\frac{(h_2 - h_1)^{2n+1}}{2n+1}\right]$$

(5.25)

$$I_5 = \int_{h_1}^{h_2} N(x_3)x_3^2 dx_3 = \frac{1}{(h_2 - h_1)^n}\left[\frac{(h_2 - h_1)^{n+3}}{n+3} + h_1\frac{(h_2 - h_1)^{n+2}}{n+2} + h_1^2\frac{(h_2 - h_1)^{n+1}}{n+1}\right]$$

(5.26)

$$I_6 = \int_{h_1}^{h_2} (N(x_3))^2 x_3 dx_3 = \frac{1}{(h_2 - h_1)^{2n}}\left[\frac{(h_2 - h_1)^{2n+2}}{2n+2} - \frac{h_1(h_2 - h_1)^{2n+1}}{2n+1}\right]$$

(5.27)

Thus if the type of compositional variation is known, the bulk properties of functionally graded structures can be evaluated.

To summarize, dome shaped three layered barrier layer structure, strains as large as 0.8 % in the 3-direction i.e. in z-direction (direction of applied field) were obtained. The reason being increased dielectric constant, due to core shell grains and surface barrier layer effect. The spontaneous polarization was high due to induced stress in core shell grains (core in compression) and because of preferred domain orientation due to "macroscopic" stress. As already discussed, in the asymmetrical structure different layers have differential thermal expansion coefficient, hence the dome shape. This is the origin of macroscopic stress, in which at interface layer, the one that contracts more is in tension and layer with less expansion coefficient is in compression. Away from the interface opposite stress system exists to counter the interface stress. Due to the macroscopic stress, the part in tension will contract more in 1-direction (x-direction) and part in

compression will contract less in the same direction. Due to 90° domain switching higher strain is obtained on application of electric field, mechanism being similar to RAINBOW.

Chapter 6

Conclusion

This study has shown that the dielectric constant of $BaTiO_3$ can be significantly increased by doping with Nd_2O_3 and ZrO_2 resulting in high strain response. Surface barrier layer structure as well as core shell microstructure can be used to give high capacitance material. Other advantages of doping are improved theoretical density, high breakdown voltage compared to barrier layer capacitors and reduced uniform submicron grain size. Reduced grain size results in smaller domains; increasing the strain response.

Moreover they are manufactured by one step sintering process, which makes processing easier compared to other high strain materials like unimorphs/bimorphs or RAINBOW. Therefore they have good prospects for actuator applications instead of environmentally hazardous lead based ceramics. Specifically following results can be highlighted:

1. Combined doping of Nd_2O_3 and ZrO_2 significantly improved dielectric properties, such as dielectric constant (20,000-35,000), low loss (tan δ<0.05), low curie temperature (~70°C) and enhanced diffuse phase transformation behavior. This was attributed to core-shell grains microstructure by isovalent ZrO_2 and BLC behavior by donor Nd_2O_3.

2. Doping of Nd_2O_3 and ZrO_2 in $BaTiO_3$ resulted in improved densities (>93% theoretical densities) and smaller and uniform submicron grain size. Smaller grain size leads to smaller ferroelectric domains enhancing strain behavior.

3. Asymmetric functionally graded $BaTiO_3$ had dome shape and was pre-stressed like RAINBOW, resulting in preferred domain orientation due to ferroelastic switching and hence high spontaneous polarization change.

4. Completely new set of equations were derived for ideal work, in converting electrical energy to mechanical energy (causing strain), which showed direct relationship between dielectric constant and spontaneous polarization change on application of electric field.

5. Finite element analysis of simplified model of functionally graded showed that there were different in-plane strains for different layers in functionally graded piezoelectric structures, resulting in bending movement.

6. The effective piezoelectric coefficient d_{31} obtained was approximately one order higher in magnitude for functionally graded $BaTiO_3$ compared to pure barium titanate.

7. The d_{33} coefficient (200×10^{-11}C/N) and spontaneous polarization change (0.177C/m^2) for 0.6 m/oNd 2wt% ZrO_2 $BaTiO_3$ was also significantly higher than pure barium titanate due to high dielectric constant and macroscopic stress.

Chapter 7

Future Work

1. Further modeling by finite element analysis.

    Finite element analysis of a material consists of dividing the volume in smaller elements by meshing; therefore by properly attributing the material properties to elements bulk properties can be evaluated.

2. Calculation of electromechanical coupling factor.

    Equations derived to relate dielectric constant and spontaneous polarization change to strain were for ideal work. There have to be some losses in conversion of electrical energy into mechanical energy. The input and output energy are related by electromechanical coupling factor. We predict that it is significantly higher for functionally graded or doped $BaTiO_3$ compared to pure barium titanate or PZT.

3. Further developing processing parameters and control.

    In order to get repeatable results further development of processing parameters and control need to be undertaken. Additional research can be done to get still better material properties.

4. Determining mechanical properties and stress generated in asymmetric structures.

    The hardness data was used to predict the mechanical properties. Finding the exact values of mechanical properties was beyond the scope of this research. Finite element analysis and other mechanical testing methods can be used to find out bulk mechanical properties. Being pre-stressed, functionally graded

BaTiO$_3$ exhibit different material properties than the compositions of different layers. Finding out stress will certainly give insight into mechanical behavior of material.

5. Determining the use as a stable actuator material

Further characterization of functionally graded BaTiO$_3$ like force generated, resonance frequency and response time need to be done for its use as stable piezoelectric actuator material.

References:

1. Suresh S and Mortensen A "*Fundamentals of Functionally Graded Materials*" (London: IOM communications) 1998.
2. Suresh S "Graded materials for resistance to contact deformation and damage *Science* --Numerical characterization of functionally graded active materials under electrical and thermal fields" 292, 2447–51, 578, 2001.
3. Suresh S, Olsson M, Giannakopoulos A, Padture N P and Jitcharoen J "Engineering the resistance to sliding-contact damage through controlled gradients in elastic properties at contact surfaces", *Acta Mater,.* 47**,** 3915–26, 1999.
4. Freund L B "Some elementary connections between curvature and mismatch strain in compositionally graded thin films" *J. Mech. Phys. Solids,* 44**,** 723–6, 1996
5. Reddy J N "Analysis of functionally graded plates" *Int. J. Numer. Methods Eng.,* 47, 663–84, 2000.
6. Suresh S, Giannakopoulos A and Olsson M "Elastoplastic analysis of thermal cycling: layered materials with sharp interfaces", *J. Mech. Phys. Solids,* 42, 979–1018, 1994.
7. Finot M and Suresh S "Small and large deformation of thick and thin-film multi-layers: effects of layer geometry, plasticity and compositional gradients", *J. Mech. Phys. Solids* 44 683–721, 1996
8. Han X, Liu G R and Lam K Y 2001 Transient waves in plates of functionally graded materials *Int. J. Numer. Methods Eng.* 52 851–65
9. Li Y, Ramesh K T and Chin E S C 2001 Dynamic characterization of layered and graded structures under impulsive loading *Int. J. Solids Struct.* 38 6045–61
10. [Butcher R J, Rousseau C-E and Tippur H V 1999 A functionally graded particulate composite: preparation, measurements and failure analysis *Acta Mater.* 47 259–68

11. Suresh S, Giannakopoulos A and Alcala J 1997 Spherical indentation of compositionally graded materials: theory and experiments *Acta Mater.* 45 1307–21
12. Nakamura T, Wang T and Sampath S 2000 Determination of properties of graded materials by inverse analysis and instrumented indentation *Acta Mater.* 48 4293–306
13. Liu G R, Han X, Xu Y G and Lim K Y 2001 Material characterization of functionally graded material by means of elastic waves and a progressive-learning neural network *Compos. Sci. Technol.* 61 1401–11
14. Liu G R, Han X and Lim K Y 2002 A combined genetic algorithm and nonlinear least squares method for material characterization using elastic waves *Comput. Methods Appl. Mech. Eng.* 191 1909–21
15. Gasik M M 1998 Micromechanicalmodeling of functionally graded materials *Comput. Mater. Sci.* 13 42–55
16. Weissenbek E, Pettermann H and Suresh S 1997 Elasto-plastic deformation of compositionally graded metal-ceramic composites *Acta Mater.* 45 3401–17
17. Starzewski M, Jasiuk I, WangW and Alzebdeh K 1996 Composites with functionally graded interphases: mesocontinuum concept and effective transverse conductivity *Acta Mater.* 44 2057–66
18. Schmauder S andWeberW 2001 Modelling of functionally graded materials by numerical homogenization *Arch. Appl. Mech.* 71 182–92
19. Pitakthangphong S and Busso E P 2002 Self-consistent elasto-plastic stress solutions for functionally graded material systems subjected to thermal transients *J. Mech. Phys. Solids* 50 695–716
20. Yamada K, Ohkubo A and Nakamura K 2001 Functional grading of a piezoelectric 1-3 composite for ultrasonic transducers with enhanced axial and lateral resolution *Proc. Symp. IEEE Ultrasonics (Atlanta, October 2001)* (Piscataway, NJ: IEEE) pp 1031–4
21. Chatterjee D K, Ghosh S K and Furlani E P 1999 Controlled composition and crystallographic changes in forming functionally gradient piezoelectric transducer *US Patent Specification* 5,900,274
22. Ruys A J, Popov E B, Sun D, Russell J J and Murray C C J 2001 Functionally graded electrical/thermal ceramic systems *J. Eur. Ceram. Soc.* 21 2025–9
23. Pei Y T and De Hosson J 2000 Functionally graded materials produced by laser cladding *Acta Mater.* 48 2617–24
24. Liu G R and Tani J 1992 SH surface waves in functionally gradient piezoelectricmaterial plates *Trans. Japan Soc. Mech. Eng.* A 58 504–7
25. Liu G R and Tani J 1994 Surface waves in functionally gradient piezoelectricmaterial plates *ASME J. Vib. Acoust.* 116 440–8
26. Zhu X, Xu J,Meng Z, Jianming Z, Zhou S, Li Q, Liu Z and Ming N 2001Microdisplacement characteristics and microstructures of functionally graded piezoelectric ceramic actuator *Mater. Des.* 21 561–6
27. Reddy J N and Cheng Z-Q 2001 Three-dimensional solutions of smart functionally graded plates *Trans. ASME, J. Appl. Mech.* 68 234–41

28. Ng T Y, He X Q and Liew K M 2002 Finite element modeling of active control of functionally graded shells in frequency domain via piezoelectric sensors and actuators *Comput. Mech.* 28 1–9

29. Lim C W and He L H 2001 Exact solution of a compositionally graded piezoelectric layers under uniform stretch, bending and twisting *Int. J. Mech. Sci.* 43 2479–92

30. Almajid A, Taya M and Hudnut S 2001 Analysis of out-of-plane displacement and stress field in a piezocomposite plate with functionally graded microstructure *Int. J. Solids Struct.* 38 3377–91

31. Uchino, K., *Ferroelectric Devices*. New York: Marcel Decker (2000).

32. Bryzek, J., Peterson, K and McCully, W : IEEE spectrum, No.5, p.20 (1994)

33. Egawa S., Niino, T., and Higuchi, T., Proc 1991 IEEE workshop on Micro electromechanical Systems, P.9 (1991)

34. Bharati, V, Xu, H.S., Shanti, G., Zhang, Q.M. and Liang K., J. Appl. Phys., 87, 452 (2000)

35. Smith W.A., Proc. IEEE Ultrasonic Symposium 755 (1989).

36. Bauer,S, Proc. Int'l. Symp. Smart Actuators,ICAT/Pennstate,PA (April 1999)

37. Eric Burscu, G. Ravicahndran and K. Bhattacharya, "Mechanics of large electrostriction in ferroelectrics", Smart Structures and Materials, Proc. SPIE, 3992, 2000

38. S.E. Park and T.R. Shrout, "Utrahigh strain and piezoelectric behavior in relaxor based ferroelectric single crystals", J. Appl. Phys. 82, pp 1804-1808, 1997

39. Uchino, K. and Jayne R. Giniewicz, "Micromechatronics", New York: Marcel Decker, 2003.

40. Piezoelectric actuators and Utrasonic Motors, Kenji Uchino, Kluwer Academic Publishers (1997)

41. Wongduan Maison, Reinhard Kleeberg, Robert B. Heimann, and Sukon Phanichphant,"*Phase Content, Tetragonality, and Crystallite Size of Nanoscaled Barium TitanateSynthesized by The Catecholate Process: effect of calcinations temperature,*" Journal of the European Ceramic Society, 23, 127-132 (2003).

42. L. L. Hench and L. K. West, Principles of Electronic Ceramics, (John Wiley & Sons, Inc., 1990), pp244-247.

43. Goldschmidt, V. M., *"Skrifter Norske Videnskaps-Akad,"* Oslo, I: Mat. -Naturv. Kl., 2.8 (1926).

44. http://cst-www.nrl.navy.mil/lattice/struk/perovskite.html.

45. Bernard Jaffe, William R. Cook, Jr., and Hans Jaffe, Piezoelectric Ceramics, (Academic Press Limited, 1971), pp49-51.

46. ibid pp 50, 184-186, 914-915.

47. W. D. Kingery, H. K. Bowen, and D.R. Uhlmann, Introduction to Ceramics, 2nd ed (John Wiley & Sons, New York), pp 913-973.

48. W. D. Kingery, H. K. Bowen, and D.R. Uhlmann, op cit, pp926-927.

49. A. J. Moulson and J. M. Herbert, op cit, p243.

50. Jaffe, B., Cook, W. R. and Jaffe, H., "Piezoelectric Ceramics", Academic Press, London, 1971.
51. Park E., "Dielectric and strain effects of core-shell/barrier layer structures in modified Barium Titanate ceramics", Phd dissertation, University of Cincinnati, 2002
52. Cross. L.E., "Ferroelectric materials for electromechanical transducer applications", Jpn. J. Appl. Physics, Pt. !, 34, pp. 2525-2532, 1995.
53. Lynch C.S., "The effect of Uniaxial stress on the electro-mechanical response of 8/65/35 PLZT", Acta. Mater. 44, pp.4137-4148, 1996.
54. Chen W. and Lynch C. S. "A micro-mechanical model for polarization switching of ferroelectric materials", Acta mater., 46, pp.5303-5311, 1998.
55. Vervey E.J.W., Haaijman D.W., Romeijn, F.C. and Van Oosterhaut, G.W., "Controlled valency semiconductors", Phillips Res. Repts., 5 ,173-87, 1950.
56. Heywang, W., "Semiconducting Barium Titanate", J. Mater. Sc., 6, 1214-26, 1971.
57. Heywang, W., "Resistivity anamoly in doped Barium Titanate", J. Am. Ceram. Soc., 47[10], 484-90, 1964.
58. Berglund C.N. and Braun H.J., "Optical absorption in single domain ferroelectric barium titanate", Phillips Res. Repts., 164[2] ,790-9, 1978.
59. Ihrig H., "On the polaron nature of the charge transport in $BaTiO_3$", Solid State Phys., 9, 3469-74, 1976.
60. Chiang, Y. M., Birnie D. and Kingery W.D., "Physical Ceramics", John Wiley and Sons, Inc., 1997.
61. Goodman G., "Ceramic Capacitor Materials";chp 2 in ceramic Materials for Electronics Edited by Relva C. Buchanan, Marcel Dekker, New York, 1986.
62. Enomoto, Y, and Yamaji, A., "Preparation of Uniformly small grained $BaTiO_3$" Am. Ceram. Soc. Bull.,60 [5] 566-70 (1981).
63. Kahn M., effects of sintering and Grain Growth reactions on the distribution of Niobium addition in Barium Titanate ceramics", PhD. Thesis, Pennsylvania state university, PA,1969.
64. Heywang W., and Kniepkamp H., "Depolarization effects in polycrystalline $BaTiO_3$", Z. Angew Physics, 6, 385-90,1954.
65. Vest R.W., Shaikh A.S. and Vest G.M.,"Dielectric properties of ultrafine grained BaTiO3,"IEEE Int. Symp. Appl. Ferroelectrics, 6th,126-129,1986.
66. Jonker G.H. and Noorlander W.," Grain Size of sintered Barium Tiatnate",Science of Ceramics 1, Edited by G.H. Stewart, Academic Press London, 1962.
67. Sharma N.C. and McCartney, E.R., "The dielectric properties of Barium titanate as function of Grain Size", J. Aust. Ceram. Soc. 10[16], 16-20, 1974.
68. Arlt G., Hennings D. and De With. G., "Dielectric Properties of Fine grained Barium Titanate Ceramics" J. Appl. Phy., 58[4], 1619-25,1985.
69. Rawal, B.S., Kahn, M., and Bausseum, W.R., "Grain core-shell structure in barium titanate based dielectric", Am. Ceram. Soc.,pp 172-188, 1981

70. Armstrong T.R. and Buchanan R.C.," Influence of core shell grains on the internal stress state and permittivity response of zirconia modified barium titanate", J. Am. Ceram. Soc., 1268-1273,1990.

71. Lu.H.Y., Bow, J.S., and Deng, W.H.,"Core-shell structures in ZrO_2-modified $BaTiO_3$ ceramic", J. Am. Ceram. Soc., 73, 3563-3568, 1990.

72. Albertsen, K., Hennings D., and Steigelmann O.,"Donor-accepter charge complex formation in Barium Titanate ceramics: Role of firing atmosphere," J. Electroceramics, 2:3, 193-198,1998.

73. Li G., Furman E. and Haertling,"Stress-enhanced displacement in PLZT Rainbow actuators,"J. Am. Ceram. Soc., 80[6], 1382-88, 1997.

74. Wang Q. M. and Cross L.E., " Analysis of high temperature reduction processing of Rainbow actuator", Materials chemistry and physics 58, 669-673,1999.

75. E. Burcsu, G. Ravichandran, K. Bhattacharya. Large electrostrictive actuation of barium titanate single crystals J. Mech. Phys. Solids 52: 823-846, 2004.

76. Stratton, J. A., Electromagnetic Theory. McGraw-Hill, London, 1941.

77. Maugin, G. A., Continuum Mechanics of Electromagnetic Solids. North-Holland, Amsterdam, 1988.

78. Hwang, S.C. and Waser R.,"Study of Electrical and mechanical contribution to switching in Ferroelectric/Ferroelastic polycrystals", Acta mater. 48, 3271-3282, 2000.

79. Jinhao Q., JHunji T., Toshiyuki U., Teppei M., Hirofumi T. and Hejun D., "Fabrication and high durability of functionally graded piezoelectric bending actuators", Smart Materials and Structures,115-121, 2003.

80. Joshi S., Mukherjee A. and Schmauder S.," Numerical characterization of functionally graded active materials under electrical and thermal fields" Smart Mater. Struct. 12, 571–579, 2003